DEVELOPMENTAL NEUROSCIENCE

Interferon-γ signaling in human iPSC–derived neurons recapitulates neurodevelopmental disorder phenotypes

Katherine Warre-Cornish[1,2]*, Leo Perfect[1,2]*, Roland Nagy[1,2], Rodrigo R. R. Duarte[3,4], Matthew J. Reid[1,2], Pooja Raval[1,2], Annett Mueller[5], Amanda L. Evans[5], Amalie Couch[1,2], Cédric Ghevaert[5], Grainne McAlonan[2,6], Eva Loth[2,6], Declan Murphy[2,6], Timothy R. Powell[3,4], Anthony C. Vernon[1,2], Deepak P. Srivastava[1,2†], Jack Price[1,2,7†]

Maternal immune activation increases the risk of neurodevelopmental disorders. Elevated cytokines, such as interferon-γ (IFN-γ), in offspring's brains play a central role. IFN-γ activates an antiviral cellular state, limiting viral entry and replication. Moreover, IFN-γ is implicated in brain development. We tested the hypothesis that IFN-γ signaling contributes to molecular and cellular phenotypes associated with neurodevelopmental disorders. Transient IFN-γ treatment of neural progenitors derived from human induced pluripotent stem cells increased neurite outgrowth. RNA sequencing analysis revealed that major histocompatibility complex class I (MHCI) genes were persistently up-regulated through neuronal differentiation—an effect that was mediated by IFN-γ–induced promyelocytic leukemia protein (PML) nuclear bodies. Critically, IFN-γ–induced neurite outgrowth required both PML and MHCI. We also found evidence that IFN-γ disproportionately altered the expression of genes associated with schizophrenia and autism, suggesting convergence between genetic and environmental risk factors. Together, these data implicate IFN-γ signaling in neurodevelopmental disorder etiology.

INTRODUCTION

Multiple lines of evidence point to immune activation during fetal development as an important risk factor for neurodevelopmental disorders (*1*). Epidemiological studies consistently find an association between maternal infection during pregnancy and increased risk of autism spectrum disorder (ASD) and schizophrenia (SZ) (*2*–*5*). Animal studies have shown that induction of an antiviral immune response during pregnancy using the double-stranded RNA mimetic polyinosinic:polycytidylic acid (poly(I:C) leads to behavioral abnormalities in offspring that are thought to be relevant to neuropsychiatric disorders. These include repetitive behavior, decreased social interactions, deficits in prepulse inhibition, and altered cognition (*6*). In parallel, transcriptomic studies of both ASD and SZ post-mortem brain tissue consistently show enrichment for inflammatory and innate immune genes (*7*–*10*). Nonetheless, the pathological mechanisms through which transient inflammatory activation increases susceptibility to neurodevelopmental disorders remain unclear.

A potential mechanistic link between maternal immune activation and neurodevelopmental disorders is the exposure of the developing brain to inflammatory cytokines. Among the inflammatory cytokines up-regulated during maternal immune activation (*11*), interferon-γ (IFN-γ) is of particular interest. It is an activator of innate cellular antiviral signaling and transcription programs whose primary function is to defend the cell against viral infection (*12*). Mid-pregnancy maternal serum IFN-γ is increased during gestation of offspring with ASD (*13*), and circulatory IFN-γ levels are elevated in neonates subsequently diagnosed with ASD relative to developmental delay controls (*14*). Intriguingly, within the brain, many antiviral IFN-γ signaling targets also play important roles in neuronal development and synaptic activity, independent of microbial infection (*15*, *16*). More recently, IFN-γ has also been described to play a role in social behavior in rodents through modulation of inhibitory neuronal GABAergic tone (*17*). Thus, it is now emerging that IFN-γ has a physiological role beyond its antiviral and immune actions.

Previous studies have shown that antiviral activation establishes enduring cellular changes that persist beyond the acute inflammatory response. Exposure to IFN-γ primes cells to induce an enhanced transcriptional response upon restimulation, allowing cells to mount a faster and more effective antiviral response (*18*, *19*). Examination of transcriptional priming at the major histocompatibility complex (MHC) locus revealed a critical role for antiviral promyelocytic leukemia protein (PML) nuclear bodies (*19*). MHC class I (MHCI) gene expression has also been shown to be persistently up-regulated in developing neurons following gestational poly(I:C) exposure in rodents (*20*). In the brain, seemingly independently of their antiviral functions, both PML and MHCI proteins play important roles in many aspects of neuronal development and function, including neurite outgrowth and axon specification (*15*), synaptic specificity (*16*), synaptic plasticity (*21*), and cortical lamination (*22*). All of these processes have been shown to be altered following gestational poly(I:C) exposure in rodents (*6*, *11*, *20*, *23*). Thus, PML nuclear bodies and MHCI proteins may link antiviral inflammatory activation to neuronal abnormalities. However, the impact of this pathway on neurodevelopment following inflammatory activation has never been examined.

In this study, we explore the hypothesis that IFN-γ–induced antiviral signaling perturbs neurodevelopmental processes associated with neurodevelopmental disorders. We used human induced pluripotent stem cells (hiPSCs) to investigate how transient IFN-γ exposure

[1]Department of Basic and Clinical Neuroscience, Institute of Psychiatry, Psychology and Neuroscience, King's College London, London, UK. [2]MRC Centre for Neurodevelopmental Disorders, King's College London, London, UK. [3]Social, Genetic and Developmental Psychiatry Centre, Institute of Psychiatry, Psychology and Neuroscience, King's College London, London, UK. [4]Division of Infectious Diseases, Weill Cornell Medicine, Cornell University, New York, NY, USA. [5]Wellcome-MRC Cambridge Stem Cell Institute, University of Cambridge, Cambridge, UK. [6]Department of Forensic and Neurodevelopmental Sciences, King's College London, London, UK. [7]National Institute for Biological Standards and Control, South Mimms, UK.
*These authors contributed equally to this work.
†Corresponding author. Email: deepak.srivastava@kcl.ac.uk (D.P.S.); jack.price@kcl.ac.uk (J.P.)

affects developing human neurons. We demonstrate that exposing hiPSC-derived neural progenitor cells (NPCs) to IFN-γ led to increased neurite outgrowth in hiPSC neurons, similar to a phenotype observed in hiPSC neurons from individuals with ASD (*24*–*26*). RNA sequencing was used to characterize the acute and persistent transcriptomic responses to IFN-γ. We observed that IFN-γ responding genes were enriched for those with genetic association to ASD and SZ. Moreover, these genes overlapped significantly with those differentially expressed in the brains of individuals with these disorders. Genes of the MHCI protein complex were acutely and persistently up-regulated. This was accompanied by an enduring increase in MHCI protein levels and PML body numbers. Critically, both PML and MHCI proteins were required for IFN-γ-dependent effects on neuronal morphology. Together, these findings highlight a potential mechanism through which antiviral signaling could contribute to intrinsic neuronal phenotypes in neurodevelopmental disorders.

RESULTS

IFN-γ increases neurite outgrowth in a hiPSC model of neurodevelopment

We and others have previously observed alterations in the morphology of hiPSC neurons derived from individuals with ASD (*24*–*26*). Since inflammatory mechanisms have been implicated in both neural development and neurodevelopmental pathology, we hypothesized that activation of antiviral signaling pathways influences the development of neuronal architecture. To investigate this, we used hiPSC-NPCs from three typically developing male individuals with no history of psychiatric illness [M1, M2, and M3; table S1 and fig. S1; (*27*, *28*)] and treated these cells with IFN-γ (25 ng/ml) daily on days (D) 17 to 21 of differentiation. Subsequently, IFN-γ was excluded from cell culture media, and neuronal differentiation was continued, resulting in post-mitotic hiPSC neurons (Fig. 1A and fig. S1). Cells were fixed on D26, D30, D35, and D40 and stained for βIII-tubulin

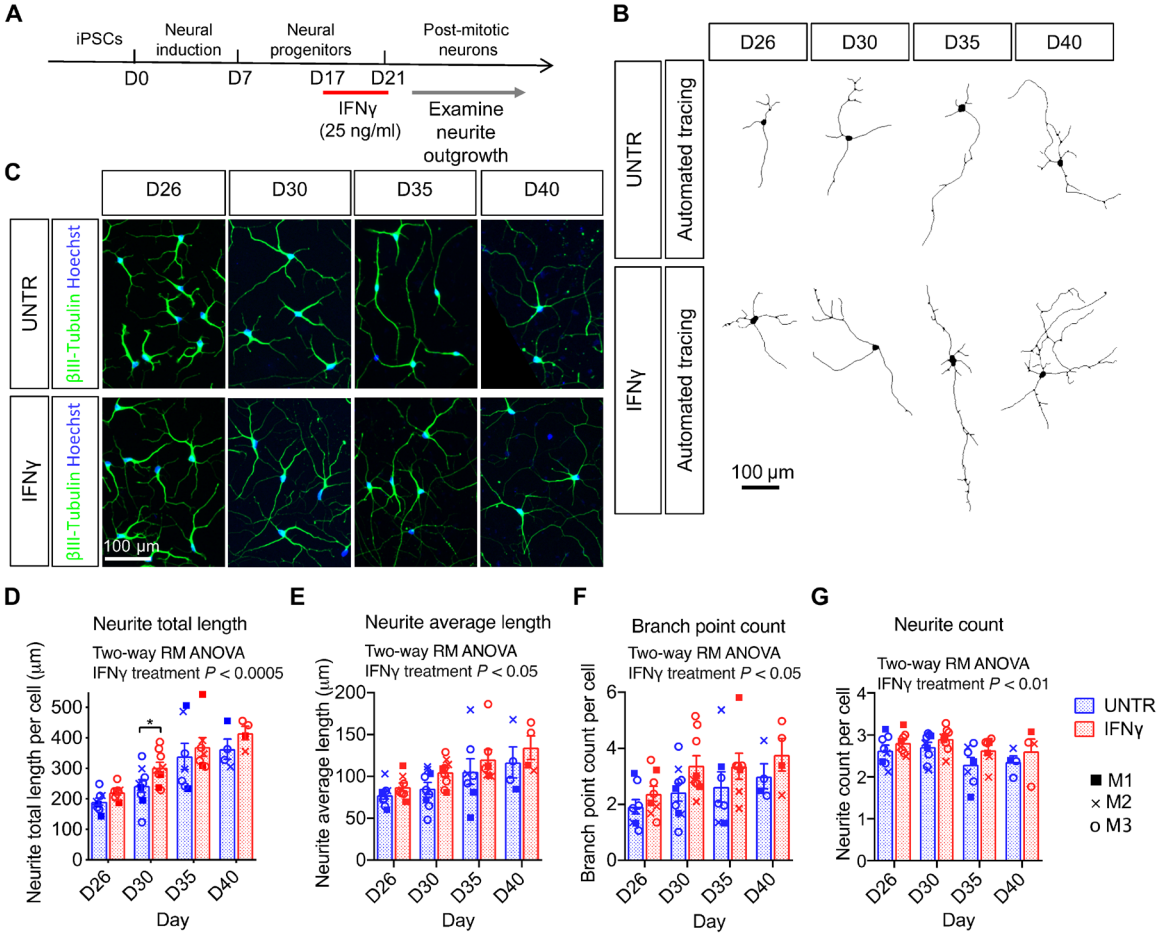

Fig. 1. IFN-γ treatment of NPCs leads to enhanced neurite outgrowth in post-mitotic neurons. (**A**) Schematic representation of the experimental timeline of iPSC differentiation and IFN-γ treatment strategy. NPCs received IFN-γ (25 ng/ml) daily in cell culture media from D17 to D20 before terminal plating on D21 and examination of neurite outgrowth. (**B**) Automated tracing of βIII-tubulin–stained neurites on D26, D30, D35, and D40 untreated (UNTR) and IFN-gamma treated cells carried out with CellInsight high content screening operated by HCS Studio Software. (**C**) Fluorescence images of βIII-tubulin and Hoechst staining acquired with CellInsight. (**D** to **G**) Graphs show the time courses of neuronal morphological properties including neurite total length per cell (D), neurite average length per cell (E), branch point count per cell (F), and neurite count per cell (G) in three control male cell lines, M1, M2, and M3. D26 untreated: $n = 8$ independent biological replicates, 6382 cells analyzed; D26 IFN-γ: $n = 8$ independent biological replicates, 7122 cells analyzed; D30 untreated: $n = 9$ independent biological replicates, 5651 cells analyzed; D30 IFN-γ: $n = 9$ independent biological replicates, 7741 cells analyzed; D35 untreated: $n = 7$ independent biological replicates, 4250 cells analyzed; D35 IFN-γ: $n = 7$ independent biological replicates, 4733 cells analyzed; D40 untreated: $n = 4$ independent biological replicates, 2792 cells analyzed; D40 IFN-γ: $n = 4$ independent biological replicates, 2872 cells analyzed. Data generated with CellInsight high content screening operated by HCS Studio Software. Results are presented as means ± SEM. Two-way RM ANOVA with Sidak's multiple comparison adjustment method. *$P < 0.05$.

(Tuj1), and high content automated neurite tracing was carried out (Fig. 1, B and C). Total neurite length measurements were averaged for each biological replicate for all three hiPSC lines. A repeated measures (RM) two-way analysis of variance (ANOVA) was performed, pairing untreated and IFN-γ-treated samples from each biological replicate. The main effects of both IFN-γ treatment and days in culture were associated with a significant increase in total neurite length per cell across the time course examined (IFN-γ treatment: $F_{1,24} = 17.02$, $P = 0.0004$; days in culture: $F_{3,24} = 12.07$, $P < 0.0001$; Fig. 1D). After demonstrating the effect of IFN-γ on neurite outgrowth across the entire dataset, we used Sidak's multiple comparison adjustment to compare individual time points. This revealed a significant increase in total neurite length in IFN-γ-treated lines at D30 ($P = 0.010$). We did not observe a significant interaction between IFN-γ treatment and time in culture (interaction of treatment × time point: $F_{3,24} = 0.60$, $P = 0.62$), indicating that both factors influence neurite outgrowth independently of each other.

We next examined whether IFN-γ-treated cells had differences in branching, neurite length, and neurite number. Previous studies of cells from individuals with ASD have reported increases in these morphological parameters (*24*–*26*). IFN-γ treatment led to a significant increase in average neurite length per cell across the time course (IFN-γ treatment: $F_{1,24} = 5.07$, $P = 0.034$; days in culture: $F_{3,24} = 6.25$, $P = 0.0027$; Fig. 1E), although Sidak's multiple comparison adjustment showed no significant difference between IFN-γ and untreated cells at individual time points ($P > 0.05$). Branch point count per cell was also higher in IFN-γ-treated cells across the time course (IFN-γ treatment: $F_{1,24} = 7.22$, $P = 0.013$; days in culture: $F_{3,24} = 2.72$, $P = 0.067$; Fig. 1F), although, similarly, no significant difference was observed with treatment at individual time points. The neurite count per cell was also higher among IFN-γ-treated neurons but did not change significantly across the time course (IFN-γ treatment: $F_{1,24} = 7.84$, $P = 0.0099$; days in culture: $F_{3,24} = 2.71$, $P = 0.068$; Fig. 1G). Again, we observed no significant difference in neurite count per cell between IFN-γ and untreated cells at individual time points. No interaction effects were observed between these morphological features and time in culture, indicating that treatment and days in culture were affecting neurite morphology independently. Together, these data indicate that exposing hIPSC-NPCs to IFN-γ results in an increase in neurite outgrowth due to longer, more numerous neurites and increased branching in hIPSC-derived neurons compared to untreated controls. These observations are consistent with previous findings in autism-derived neuronal cells and indicate a potential disruption in the development of early neuronal morphology (*24*–*26*).

Transcriptomic analysis of IFN-γ exposure during neuronal differentiation

After demonstrating the effect of IFN-γ on early neuronal morphology, we sought to explore the mechanisms that underlie these effects. We carried out RNA sequencing analysis of the same three hiPSC lines (M1, M2, and M3; table S1) to examine the transcriptomic changes caused by IFN-γ treatment of human NPCs and neurons. The experiment had six conditions and is schematized in Fig. 2A. We sought to capture (i) the acute response of NPCs to IFN-γ, (ii) the acute response of neurons to IFN-γ, (iii) the persistent response of neurons after IFN-γ exposure at the NPC stage, and (iv) the effect of repeated IFN-γ exposure at the NPC and neuronal stages. Principal components analysis revealed that the largest source of variation across the dataset corresponded to cell type, with the first principal component explaining 72% of variance and separating NPCs and neurons (Fig. 2B). The second principal component segregated the samples by IFN-γ exposure and described 20% of the observed variance between samples.

Differential gene expression analysis was performed using DESeq2 (*29*). We found 1834 differentially expressed genes (DEGs) by comparing untreated and treated NPCs [18 U versus 18 T, Wald test, false discovery rate (FDR) < 0.05; Fig. 2, C and D]. The comparison of untreated and treated neurons revealed 751 DEGs (30 UU versus 30 UT; Fig. 2, C and E). There were 464 DEGs in common between the two comparisons (fig. S2A). The canonical IFN-γ signaling pathway was activated in both NPCs and neurons, resulting in significant up-regulation of *JAK2*, *STAT1*, *STAT2*, and downstream IFN-stimulated genes such as *IRF1* (Fig. 2, D and E). Up-regulated genes were highly enriched for the Gene Ontology (GO) term "IFN-γ-mediated signaling pathway" (9-fold in NPCs and 14-fold in neurons; FDR = 4.47×10^{-21} and 2.68×10^{-23}, respectively; Fig. 2H). Genes belonging to the MHCI complex (GO term "MHCI protein complex") were overrepresented in the up-regulated genes (11-fold in NPCs and 21-fold in neurons; FDR = 8×10^{-4} and 3.98×10^{-5}, respectively; Fig. 2H) and among the highest ranked DEGs in NPC and neurons treated with IFN-γ (Fig. 2, D and E). We also found that the genes down-regulated by treated neurons were enriched twofold for the GO term "plasma membrane" (FDR = 0.002). Full differential expression and GO results are reported in tables S2 and S3, respectively.

The persistent transcriptional response to IFN-γ was of interest given the enduring impact of IFN-γ on neuronal morphology described above. To this end, we compared untreated and pretreated neurons (30 UU versus 30 TU). Neurons exposed to IFN-γ at the NPC stage showed enduring transcriptional changes, with 26 genes significantly up-regulated and 2 genes downregulated in post-mitotic neurons 9 days after treatment (Fig. 2F). Notably, the up-regulated gene set was highly enriched for MHCI genes, with the GO term MHCI protein complex enriched 357-fold (FDR = 3.33×10^{-8}; Fig. 2H). The top five ranked DEGs were all involved in MHCI antigen presentation. Also of interest, the metabotropic glutamate receptor gene *GRM3* was up-regulated, while the GABAergic transcription factor gene *LHX6* was down-regulated in pretreated neurons (Fig. 2F).

We also found evidence of IFN-γ-induced cellular priming, where repeated exposure at the NPC and neuronal stages (30 TT) induced considerably more DEGs than a single neuronal treatment (30 UT) when compared to untreated neurons (30 UU). This double hit induced 1091 DEGs, 45% more than were detected after a single neuronal treatment (Fig. 2G and fig. S2B). This is consistent with previous reports of IFN-γ-induced transcriptional priming (*18*, *19*). The genes down-regulated by neurons that received a double hit were enriched fourfold for the GO term "synapse" (FDR = 0.049). Together, these results demonstrate that IFN-γ exposure induces widespread and persistent transcriptional changes during human neuronal differentiation. Considering their previously proposed role in neurite outgrowth in mouse (*15*, *30*), these data highlight MHCI proteins as candidates to explain the IFN-γ-induced morphological phenotype described above.

IFN-γ disproportionately alters SZ and ASD risk genes

Viral infection has previously been linked with neurodevelopmental and psychiatric disorders (*1*). Therefore, we examined whether SZ- and ASD-associated genes were disproportionately altered in NPCs and neurons upon exposure to IFN-γ. We first performed gene set enrichment analysis using MAGMA (*31*) to test for overlap with

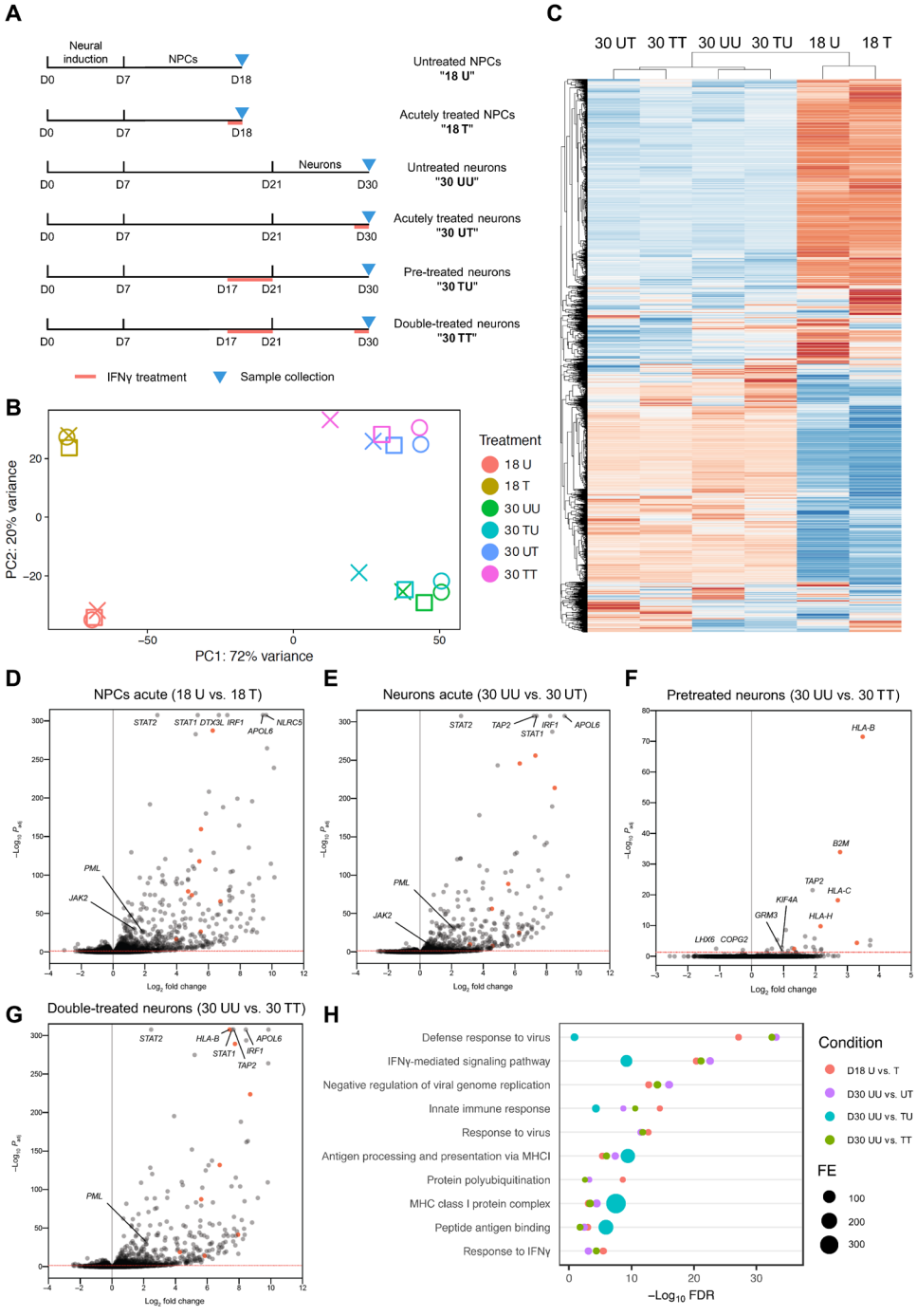

Fig. 2. RNA sequencing analysis reveals a widespread and persistent transcriptomic response of human NPCs and neurons to IFN-γ. (**A**) Schematic representation of the experimental conditions. (**B**) Principal components analysis biplot of all samples. The first principal component segregates conditions by time point, while the second separates conditions by recent treatment. Cell lines are represented by point shape: M1 = square, M2 = cross, M3 = circle. PC, principal component. (**C**) Heatmap of all DEGs clustered by row and column. Replicates are collapsed by condition. (**D** to **G**) Volcano plots with selected genes annotated. The dotted red line represents the threshold for statistical significance of $P_{adj} = 0.05$. Red dots identify genes of the MHCI protein complex. (**H**) Cleveland plot of selected enriched GO terms from the up-regulated gene sets illustrating statistical significance and fold enrichment (FE).

genes associated with SZ by a recent genome-wide association study (GWAS) (*32*). Variants corresponding to the MHC locus were excluded due to complex linkage disequilibrium in the region. The analysis revealed that SZ genes overlapped with genes down-regulated upon IFN-γ exposure in NPCs (18 U versus 18 T; β = 0.14, SD = 0.024, $P = 0.002$, FDR = 0.007) and neurons (30 UU versus 30 UT; β = 0.42, SD = 0.026, $P = 0.002$, FDR = 0.007). No enrichment was observed in the up-regulated gene sets. Additional analysis was carried out

using an SZ risk gene list compiled by the PsychENCODE Consortium by linking GWAS loci to potential disease genes using integrated regulatory networks (*33*). Consistent with the MAGMA analysis, the PsychENCODE list was enriched in the gene set down-regulated by NPCs in response to IFN-γ [Fisher's exact test, odds ratio (OR) = 1.7, FDR = 0.023; Fig. 3A]. Genes in this group included *GRIN2A*, *PRKD1*, and *TSNARE1* (fig. S3A). This list was also enriched in the gene set up-regulated by neurons in response to IFN-γ (OR = 1.7, FDR = 0.027; Fig. 3A). Notable genes in this group included *TCF4*, *ATXN7*, and *ZNF804A* (fig. S3B).

Similar analyses were carried out to investigate the association between IFN-γ signaling and ASD risk genes. MAGMA analysis did not reveal enrichment of common risk variants identified by the largest GWAS for ASD carried out to date ($P > 0.05$) (*33*). Given the fact that ASD GWAS are relatively underpowered and that this analysis neglects the contribution of rare variants, we also tested for overlap with ASD risk genes from the Simons Foundation Autism Research Initiative (SFARI) database (*34*). The SFARI database is a manually curated list of ASD risk genes scored by the strength of evidence. Category 1 to 4 risk genes were significantly overrepresented in the gene set down-regulated by NPCs in response to IFN-γ (OR = 1.7, FDR = 0.037; Fig. 3A), which included genes commonly associated with ASD such as *NLGN3*, *SHANK2*, *UPF3B*, and *NRXN3* (fig. S4). After restricting the analysis to a subset of higher confidence, category 1 and 2 genes, the enrichment was no longer statistically significant. Neither of the SFARI gene lists overlapped with the up-regulated gene sets from NPCs or neurons. Collectively, these data suggest that IFN-γ exposure during human neuronal differentiation disproportionately alters genes associated with SZ and ASD.

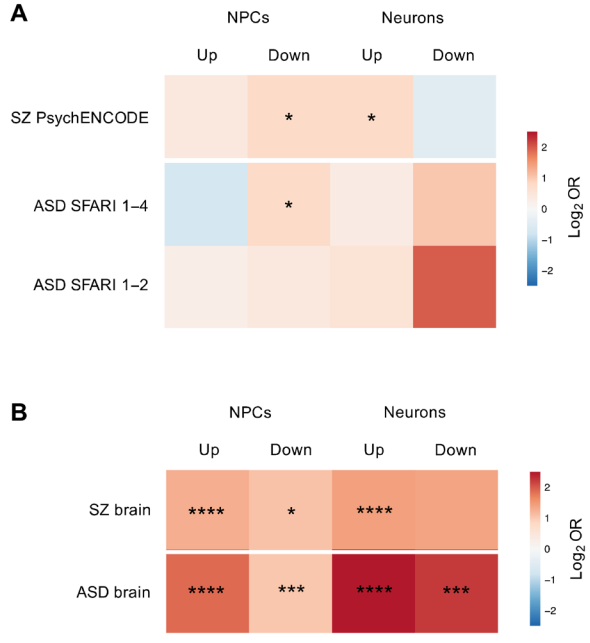

Fig. 3. Relevance of IFN-γ-dependent gene expression changes to SZ and ASD. (**A**) Enrichment of SZ and ASD risk genes and (**B**) DEGs detected in the brains of patients with SZ and ASD among our IFN-γ-responding genes. Log_2 odds ratio (OR) is represented by color and statistical significance is indicated by asterisks (*FDR < 0.05, ***FDR < 0.001, and ****FDR < 0.0001). Fisher's exact test BH corrected for multiple comparisons.

IFN-γ response recapitulates the transcriptomic signatures observed in SZ and ASD brains

Overlap between IFN-γ-responding genes and those found to be differentially expressed in the post-mortem brains of individuals with SZ and ASD would corroborate the role of IFN-γ signaling in neurodevelopmental disorders. We used data from the PsychENCODE cross-disorder study, the largest transcriptome-wide analysis of SZ and ASD brains carried out to date (*10*). We found a highly significant enrichment of genes from both disorders (Fig. 3B). More specifically, there was a significant overlap between genes up-regulated (OR = 2.5, FDR = 3.62×10^{-15}) and down-regulated (OR = 2.1, FDR = 0.012) in NPCs in response to IFN-γ with those up- and down-regulated in the post-mortem brains of individuals with SZ. We also report a significant overlap between genes up-regulated by neurons in response to IFN-γ with those up-regulated in the brains of patients with SZ (OR = 2.7, FDR = 1.98×10^{-11}). Next, we tested for overlap with genes found to be differentially expressed in the post-mortem brains of individuals with ASD. Again, there was a significant overlap between genes up-regulated (OR = 3.7, FDR = 2.26×10^{-21}) and down-regulated (OR = 2.0, FDR = 2.82×10^{-4}) in NPCs. The effect was even more pronounced for genes up-regulated (OR = 5.6, FDR = 1.39×10^{-25}) and down-regulated (OR = 4.6, FDR = 3.80×10^{-4}) in neurons. The overlapping up-regulated genes at both time points in both disorders were enriched for GO terms including IFN-γ-mediated signaling pathway and "defense response to virus" (table S4). These results indicate that IFN-γ signaling modifies gene expression in a manner consistent with the dysregulation observed in the brains of individuals with SZ and ASD.

Regulation of MHCI genes by PML nuclear bodies

The RNA sequencing analysis described above revealed an acute and persistent up-regulation of MHCI genes in hiPSC neurons after exposure to IFN-γ. In non-neuronal cells, IFN-γ has been shown to induce long-lasting changes in signal-dependent transcription of MHC proteins through the formation of PML bodies (*19*). PML bodies are dynamic, DNA binding protein complexes that mediate myriad transcriptional functions from viral gene silencing (*35*) to neurogenesis (*22*) and neuronal homeostatic plasticity (*21*). Because the MHCI pathway was highly enriched in the pretreated neurons and *PML* was similarly up-regulated in acutely treated NPCs and neurons (Fig. 2, D and E), we investigated the putative role of PML bodies in mediating the effects of IFN-γ. We hypothesized that PML bodies could underlie the persistent up-regulation of MHCI following IFN-γ treatment. Cells from the six IFN-γ treatment conditions (Fig. 2A), using the three hiPSC lines, were stained for PML (Fig. 4, A and C). Acute 24-hour treatment of NPCs at D17 to D18 resulted in a significant increase in PML bodies per cell ($P < 0.0001$; Fig. 4, A and B). The increase in PML bodies persisted through differentiation and was still observed in neurons ($P < 0.0001$; Fig. 4, C and D). Conversely, treatment of post-mitotic neurons had no effect on numbers of PML bodies, with or without pretreatment at D17 to D21 (Fig. 4D). These results indicate a time window of sensitivity in neuronal differentiation, during which IFN-γ exposure leads to a persistent increase in PML bodies.

PML nuclear bodies are known to be specifically disrupted following binding of arsenic trioxide (As_2O_3) (*36*). Therefore, we pretreated NPCs with As_2O_3 from D16 to D17, followed by cotreatment with As_2O_3 and IFN-γ from D17 to D18, and then counted PML bodies per nucleus [Fig. 4, E(i) and F]. As previously observed

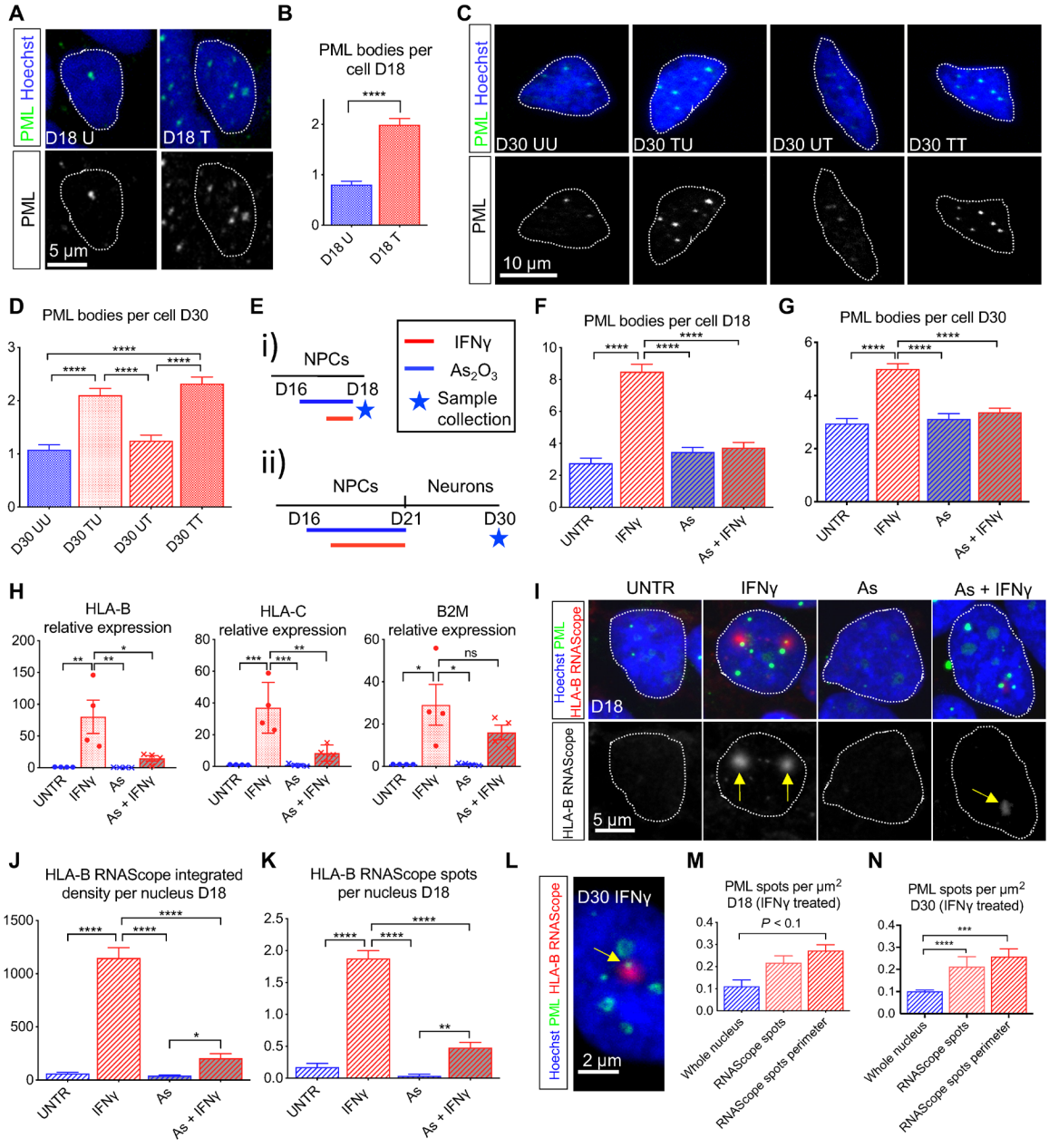

Fig. 4. PML bodies persistently increase following IFN-γ treatment, regulate MHCI gene transcription, and associate spatially with HLA-B transcription. (**A** and **B**) Increased PML nuclear body expression following acute IFN-γ treatment: D18 U, $n = 354$ cells; D18T, $n = 286$ cells. Two-tailed Mann-Whitney test. (**C** and **D**) PML body expression was persistently increased following IFN-γ treatment: D30 UU, $n = 236$ cells; D30 TU, $n = 264$ cells; D30 UT, $n = 231$ cells; and D30 TT, $n = 307$ cells. Kruskal-Wallis test with Dunn's multiple comparison adjustment. (**E**) Treatment schematic. (**F** and **G**) As_2O_3 (As) blocked IFN-γ-induced PML body expression: D18 UNTR, $n = 57$ cells; D18 IFN-γ, $n = 65$ cells; D18 As, $n = 64$ cells; and D18 IFN-γ + As, $n = 54$ cells. D30 UNTR, $n = 104$ cells; D30 IFN-γ, $n = 129$ cells; D30 As, $n = 119$ cells; and D30 As + IFN-γ, $n = 105$ cells. Kruskal-Wallis test with Dunn's multiple comparison test. (**H**) IFN-γ-induced HLA-B, HLA-C, and B2M expression is blocked by As. One-way ANOVA with Tukey's multiple comparison test. (**I** to **K**) Expression of HLA-B pre-mRNA and PML in IFN-γ-treated NPCs (D18): UNTR, $n = 57$ cells; IFN-γ, $n = 65$ cells; As, $n = 64$ cells; and IFN-γ + As, $n = 54$ cells. Kruskal-Wallis test with Dunn's multiple comparison adjustment. (**L** to **N**) Colocalization of HLA-B pre-mRNA and PML in D18 and 30 IFN-γ-treated cells: D18, $n = 67$ cells; D30, $n = 58$ cells. Kruskal-Wallis test with Dunn's multiple comparison test. Three control cell lines throughout. $^*P < 0.05$, $^{**}P < 0.01$, $^{***}P < 0.001$, and $^{****}P < 0.0001$; ns, not significant.

(Fig. 4A), IFN-γ treatment led to a notable increase in PML bodies per nucleus ($P < 0.0001$); this was blocked by cotreatment with As_2O_3. Alone, As_2O_3 had no detectable impact on the number of PML bodies. To test whether As_2O_3 treatment also prevented the persistent increase in PML bodies, the experiment was repeated, this time allowing NPCs to differentiate into neurons [Fig. 4, E(ii) and G]. Again, we observed a significant increase in PML bodies with IFN-γ treatment alone ($P < 0.0001$), which was entirely prevented by cotreatment with As_2O_3. We could thus conclude that As_2O_3 prevented both acute and persistent PML body induction by IFN-γ.

To investigate whether PML bodies were required for IFN-γ-dependent transcriptional activation of MHCI genes, we performed

quantitative polymerase chain reaction (qPCR) on NPCs from three hiPSC lines exposed to As_2O_3, IFN-γ, or combined treatment [Fig. 4E(i)]. We observed that IFN-γ-dependent induction of the MHCI genes human leukocyte antigen–B (*HLA-B*) and *HLA-C* was blocked by exposure to As_2O_3 (Fig. 4H). Induction of the MHCI receptor subunit gene *B2M* was not blocked by As_2O_3, suggesting that the PML-dependent effect is specific to MHC genes. Similarly, neither of the genes encoding IFN-γ receptor subunits, IFNGR1 and IFNGR2, were affected by As_2O_3 cotreatment (fig. S5, A and B). Collectively, these data support a model in which PML nuclear bodies mediate IFN-γ-dependent transcription of MHCI genes.

Increased expression of both *PML* and *HLA-B* has previously been shown in post-mortem brain tissue from individuals with ASD (*9*, *10*, *37*). *PML* is also up-regulated in post-mortem SZ brains (*10*). As these findings are from adult post-mortem brain tissue, it is unclear whether this signaling pathway is altered from an early developmental time point in ASD brains. To determine whether *PML* and *HLA-B* are similarly increased in hiPSC-derived neural cells in vitro, we differentiated hiPSCs from three male individuals diagnosed with ASD into NPCs, alongside the three control cell lines, as previously described (Fig. 1A and fig. S1). The individuals diagnosed with ASD were recruited from the Longitudinal European Autism Project (LEAP) (*38*). All three individuals (ASD_M1_08, 004_ASM_02, and 010_ASM_02) had a primary diagnosis of ASD (table S1). These ASD cases were considered to be idiopathic as no ASD-associated copy number variations or single-nucleotide variants were detected in these individuals. Furthermore, no serological complications were reported during gestation. We used qPCR to examine relative expression of *PML*, *HLA-B*, and *B2M* in NPCs from the three ASD and three control lines. We observed statistically significant increases in the expression of both *PML* and *HLA-B* ($P = 0.0005$ and $P = 0.0002$, respectively; fig. S6, A and B). No difference in *B2M* expression was detected ($P = 0.93$; fig. S6C). We further examined the expression of PML bodies in NPCs from the same ASD and control cell lines using immunocytochemistry (fig. S6D). We observed a significant increase in PML bodies per nucleus in the ASD NPCs relative to the control NPCs (fig. S6E). While it must be noted that these observations arise from only three ASD individuals and therefore should not be generalized, these findings suggest that increased expression of *PML* and *HLA-B* could be present in early stages of ASD neural development.

IFN-γ induces *HLA-B* transcription near PML nuclear bodies

To further interrogate the necessity of PML for IFN-γ-induced MHCI gene expression, RNA fluorescence in situ hybridization (FISH) was carried out on NPCs from three hiPSC lines treated with IFN-γ, As_2O_3, or cotreated with IFN-γ and As_2O_3 [Fig. 4, E(i)and I]. Our qPCR experiments demonstrated that IFN-γ-dependent up-regulation of *HLA-B* and *HLA-C* was similarly blocked by As_2O_3. However, as *HLA-B* demonstrated the greatest up-regulation in pretreated neurons, we focused on this MHCI gene (Fig. 2F). We used a probe specific to the pre-spliced *HLA-B* RNA transcript to tag the site of transcription. IFN-γ treatment led to a marked increase in *HLA-B* pre-mRNA ($P < 0.0001$; Fig. 4, I to K). This induction was largely prevented by cotreatment with As_2O_3 (Fig. 4, I to K), supporting the requirement for PML in IFN-γ-dependent *HLA-B* transcription. Furthermore, costaining for PML and *HLA-B* pre-mRNA revealed a positive correlation in the IFN-γ-treated condition. This was observed both as integrated density of PML and *HLA-B* expression per nucleus (slope significantly greater than zero, $P = 0.027$; fig. S7A) and as number of spots per nucleus in each channel (slope significantly greater than zero, $P = 0.0037$; fig. S7B). A significant positive correlation between PML and *HLA-B* spots per nucleus was also observed in the unstimulated condition ($P = 0.0014$; fig. S7F), although there was no correlation between the integrated density of PML and *HLA-B* ($P = 0.38$; fig. S7E). A relationship between PML bodies and IFN-γ-induced *HLA-B* transcription is thus strongly supported.

If PML bodies directly regulate MHCI gene expression, then we would predict them to be in close proximity to the site of transcription. To investigate this spatial relationship, we carried out RNA FISH using the probe described above, specific to pre-spliced *HLA-B* RNA transcript. Because splicing is highly localized (*39*), we reasoned that the site of the pre-spliced transcript could be used as a proxy for the location of transcription. Costaining for PML and *HLA-B* pre-mRNA revealed that, following IFN-γ treatment, *HLA-B* spots were frequently located immediately adjacent to, or overlapping with, PML bodies (Fig. 4L). To investigate this further, we measured the density of PML bodies (spots per micrometer) within *HLA-B* spots or *HLA-B* spot perimeters (see Materials and Methods for full definitions) and compared this to the density of PML bodies across the nucleus as a whole in IFN-γ-treated NPCs and neurons (Fig. 3, M and N, and fig S7, C and D). In IFN-γ-treated NPCs, the increased density of PML bodies in *HLA-B* pre-mRNA spot perimeters did not reach statistical significance ($P = 0.09$). However, in IFN-γ-treated neurons, a significantly higher density of PML bodies was observed in the *HLA-B* pre-mRNA spots ($P < 0.0001$) and spot perimeters ($P = 0.0007$) than the nucleus as a whole, indicating a positive spatial association. By contrast, in untreated NPCs and neurons, PML spots were never observed to overlap with *HLA-B* pre-mRNA spots or spot perimeters (fig. S7, C and D). To confirm the existence of a nonrandom spatial relationship, we carried out random shuffle nearest neighbor analysis on IFN-γ-treated NPCs (*40*). Actual distances between *HLA-B* spots and PML bodies were observed to be significantly shorter than simulated distances following randomization ($P < 0.0001$), confirming a positive spatial relationship (fig. S7, G and H). These results confirm that PML bodies are in closer proximity to the site of *HLA-B* transcription than would be expected by chance, supporting the hypothesis that PML is required for IFN-γ-induced MHCI gene transcription.

PML and MHCI mediate IFN-γ-induced neurite outgrowth

Having demonstrated a role for PML bodies in IFN-γ-induced MHCI gene transcription, we next asked whether PML and MHCI were required for the IFN-γ-dependent increased neurite outgrowth. MHCI proteins have previously been reported to be expressed during, and required for, neurite outgrowth in primary cultured rodent neurons (*15*). To examine the role of MHCI proteins in IFN-γ-induced neurite outgrowth, we first carried out instant (i) Structured Illumination Microscopy (SIM) super-resolution microscopy to determine the subcellular localization of MHCI proteins HLA-A, HLA-B, and HLA-C (Fig. 5A). We found MHCI proteins to be present in the neurites, growth cones, and cell bodies of untreated neurons. We then examined the effects of IFN-γ- and As_2O_3-induced PML disruption on MHCI abundance in neurites and growth cones in neurons from three control hiPSC lines, following the experimental outline schematized in Fig. 4E(ii). IFN-γ treatment induced a significant increase in MHCI intensity within growth cones and neurite compartments (neurites: $P = 0.0021$; growth cones: $P = 0.0012$; Fig. 5, B and C). This increase was prevented by cotreatment with As_2O_3 in both compartments ($P = 1$ for both). MHCI was enriched in growth cones relative to the associated neurite in both

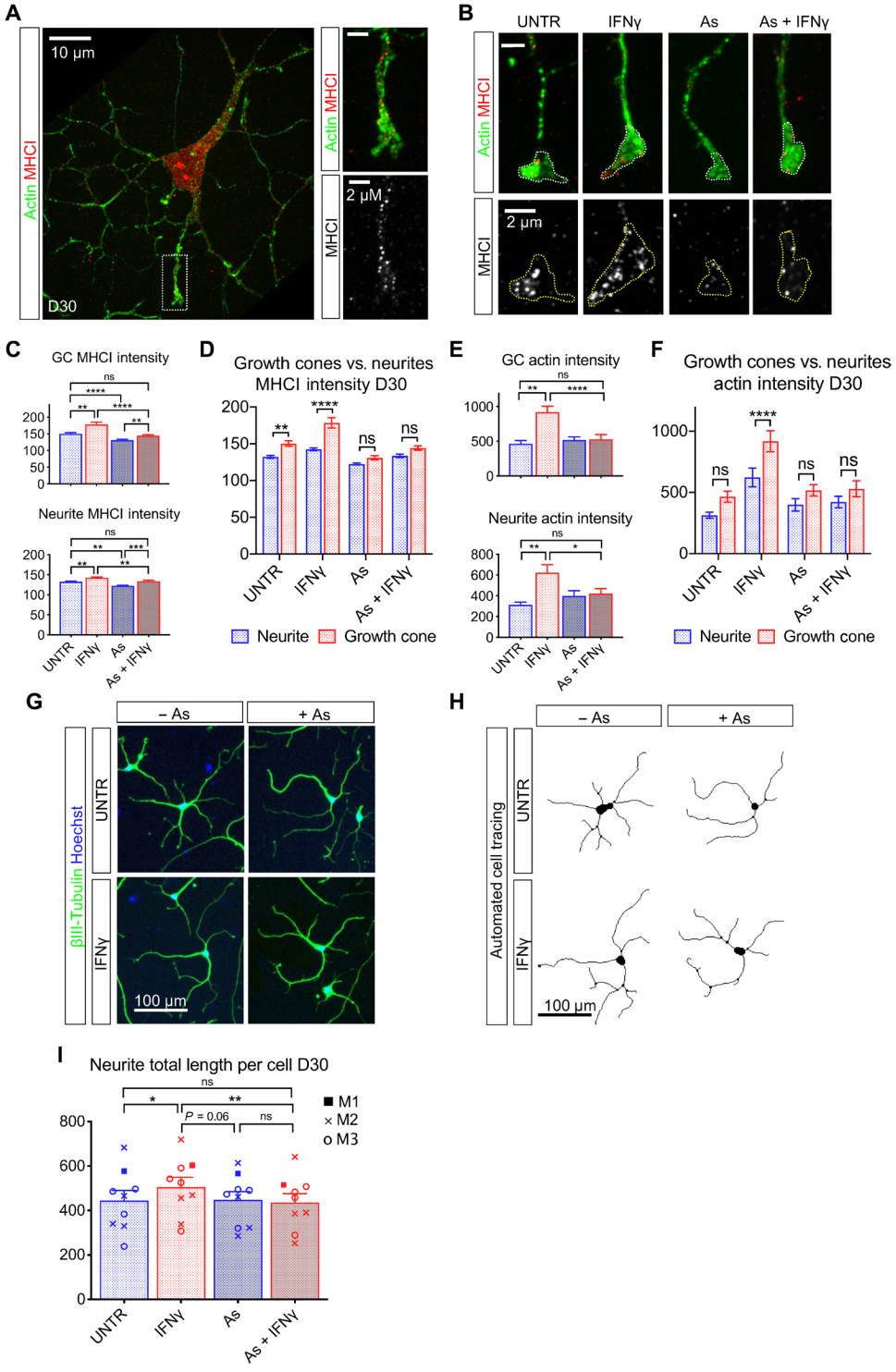

Fig. 5. MHCI proteins are enriched in neuronal growth cones in a PML-dependent manner, and disruption of PML prevents IFN-γ-dependent neurite outgrowth. (**A** and **B**) iSIM super-resolution images of actin and MHCI in D30 neurons, with MHCI observable in cell bodies, neurites, and growth cones in UNTR, IFN-γ, As, and As + IFN-γ treatment conditions. (**C** to **F**) Quantification of MHCI and actin in D30 neurons in neurites and growth cones (GC). UNTR, $n = 52$ cells; IFN-γ, $n = 82$ cells; As, $n = 55$ cells; and As + IFN-γ, $n = 59$ cells; three control cell lines. (C and E) One-way ANOVA with Tukey's multiple comparison test. (D and F) RM two-way ANOVA with Sidak's multiple comparison adjustment. (**G**) Fluorescence images of βIII-tubulin and Hoechst staining acquired with CellInsight high content screening system operated by HCS Studio Software. (**H**) Automated tracing of βIII-tubulin–stained neurites in D30 UNTR, IFN-γ, As, and As + IFN-γ conditions carried out with CellInsight high content screening system. (**I**) Graph showing neurite total length per cell in D30 UNTR, IFN-γ, As, and As + IFN-γ conditions. $n = 9$ independent biological replicates. UNTR, 5038 cells analyzed; IFN-γ, 5668 cells analyzed; As, 5169 cells analyzed; and As + IFN-γ, 3210 cells analyzed; three control cell lines. RM one-way ANOVA with Tukey's multiple comparison test. Data generated with CellInsight high content screening operated by HCS Studio Software. Results are presented as means ± SEM. *$P < 0.05$, **$P < 0.01$, ***$P < 0.001$, and ****$P < 0.0001$.

untreated ($P = 0.0034$) and IFN-γ-treated neurons ($P < 0.0001$; Fig. 5D). The enrichment of MHCI in growth cones was blocked by As_2O_3 treatment, both with and without IFN-γ (As: $P = 0.40$; As = IFN-γ: $P = 0.13$; Fig. 5D). These results support a requirement for PML-dependent signaling in the expression and appropriate subcellular localization of MHCI proteins both basally and following IFN-γ exposure.

Significantly increased actin intensity was also observed in both neurites and growth cones following IFN-γ treatment (neurites: $P = 0.0020$; growth cones: $P = 0.0021$; Fig. 5E). Cotreatment with As_2O_3 prevented this increase in both compartments ($P = 1$ for both). Actin staining intensity was also increased in growth cones relative to adjoining neurites following IFN-γ treatment ($P < 0.0001$), and this enrichment was prevented by cotreatment with As_2O_3 (As: $P = 0.57$; As + IFN-γ: $P = 0.13$; Fig. 5F). Together, these results indicate that PML-dependent IFN-γ-activated signaling pathways have a functional impact on growth cone composition and actin dynamics.

To determine whether intact PML bodies are required for IFN-γ-dependent increased neurite outgrowth, we treated NPCs with IFN-γ and As_2O_3 and then continued differentiation of these cells into post-mitotic neurons and assessed neurite outgrowth. As previously described, we observed an increase in total neurite length per cell in the IFN-γ-treated relative to the untreated neurons ($P = 0.04$; Fig. 5, G to I). This increase was prevented by cotreatment with As_2O_3 ($P = 0.98$), supporting a requirement for PML in IFN-γ-induced neurite outgrowth. These results support a model whereby IFN-γ activates PML body formation, leading to MHCI gene transcription, expression of MHCI in growth cones, and increased neurite outgrowth.

IFN-γ-mediated increase in MHCI and neurite outgrowth requires expression of B2M

To rule out nonspecific effects of As_2O_3 and confirm the requirement for MHCI in IFN-γ-dependent neurite outgrowth, we investigated the effect of blocking MHCI cell surface expression on IFN-γ-induced morphological changes. To achieve this, we took advantage of the requirement for the B2M protein for cell surface expression of MHCI (*41*). First, we sought to demonstrate that IFN-γ-induced expression of B2M protein was required for MHCI expression in our NPCs. We observed a significant increase in both B2M and MHCI expression following exposure to IFN-γ ($P = 0.0011$; Fig. 6, A to C). We then knocked down *B2M* in NPCs using a lentiviral vector containing *B2M*-targeting short hairpin RNA (shRNA) in the three control hiPSC lines. Virus containing nontargeting scrambled shRNA was used as a control. shRNA-mediated knockdown of *B2M* blocked IFN-γ-induced MHCI expression in NPCs (IFN-γ versus IFN-γ + shRNA B2M k/d, $P < 0.0001$; Fig. 6, A and C). These data confirm that B2M is required for IFN-γ-induced up-regulation of MHCI in NPCs. Next, we used a human embryonic stem cell (hESC) line, MS3 HLA null, in which the *B2M* gene has been excised using a CRISPR-Cas9 nickase approach. This results in cells lacking cell surface MHCI. We used the MS3 HLA null hESC line to further investigate whether MHCI was required for IFN-γ-induced neurite outgrowth. Five independently cultured biological replicates of MS3 HLA null hESCs were differentiated using the same neural induction protocol used with our neurons and, subsequently, treated with IFN-γ (25 ng/ml) on D17 to D21 (Fig. 1A and fig. S1). Treatment of MS3 HLA null NPCs with IFN-γ did not increase MHCI expression (B2M: $P = 0.68$; MHCI: $P = 0.34$; Fig. 6, D to F), consistent with the requirement for B2M for the expression of MHCI proteins. Critically, when we assessed neurite outgrowth in MS3 HLA null neurons following IFN-γ treatment, we no longer observed an effect of treatment on total neurite length ($P = 0.74$; Fig. 6, G and H). Together, these data demonstrate that IFN-γ-mediated alterations in neurite outgrowth require the expression of B2M and MHCI proteins (Fig. 6I).

DISCUSSION

Epidemiological and animal studies support a role for antiviral inflammatory activation in the etiology of neurodevelopmental disorders. While the molecular mechanisms that underlie this association are unclear, inflammatory cytokines are thought to play a central role (*11*). In this study, we used hiPSCs to examine the impact of IFN-γ exposure during human neuronal differentiation. Intriguingly, we observed morphological and transcriptomic changes previously associated with neurodevelopmental disorders. We propose a model where IFN-γ promotes neurite outgrowth by a PML-dependent long-lasting up-regulation of MHCI proteins at neuronal growth cones (Fig. 6I). To our knowledge, the mechanisms through which transient developmental immune activation cause lasting alterations in neuronal phenotypes have not previously been examined in a human system.

IFN-γ exposure at the neural progenitor stage increased neurite outgrowth in human neurons. This was measurable as both neurite length and branch number. Our observation is consistent with studies of mouse NPCs (*42*) and a human cancer cell line (*43*). This study is the first report of this effect in human neurons. Neurite outgrowth is a fundamental stage of neuronal maturation, where neural progenitors extend processes, which can later become axons or dendrites. However, an increase in neurite outgrowth at an early stage of development may not result in a more extensive dendritic or axonal arbor in mature neurons. Nevertheless, alterations in neurite outgrowth in the developing brain would be predicted to have implications for neuronal connectivity and ultimately brain function. Increased neurite outgrowth has been found in hiPSC neurons derived from individuals with ASD (*24*–*26*). Abnormalities in neurite outgrowth have also been observed in hiPSC neurons from patients with SZ (*44*). Note that the extent to which cultured hiPSC neurons faithfully recapitulate neuronal morphogenesis in the developing brain is unknown. Nonetheless, post-mortem studies of individuals diagnosed with ASD and SZ have pointed to abnormal cortical neuron organization, dendritic arborization, and dendritic spine density (*45*). Furthermore, the macrocephaly present in some ASD cases has been attributed to increased dendrite number and size (*46*). Offspring of pregnant dams exposed to a single gestational dose of poly(I:C) also display altered cortical development, with perturbed dendritic and synapse formation (*6*, *11*, *20*, *23*). Further evidence comes from large-scale genetic studies of ASD and SZ, which consistently identify genes encoding synaptic proteins and those involved in neuronal maturation (*33*). Thus, although a causative role has not been established, these reports suggest that disturbed neurite outgrowth may be relevant to the pathophysiology of neurodevelopmental disorders.

A key question we sought to address was how transient immune activation could have a lasting impact on neuronal phenotype. PML nuclear bodies are chromatin-associated organelles that play an important role in viral infection response and transcriptional regulation. Moreover, PML is involved in neuronal development and function (*21*, *22*). We found that IFN-γ established a long-lasting increase in PML body number during neuronal differentiation. PML bodies were spatially associated with the site of *HLA-B* transcription, and their disruption prevented IFN-γ-induced MHCI transcription.

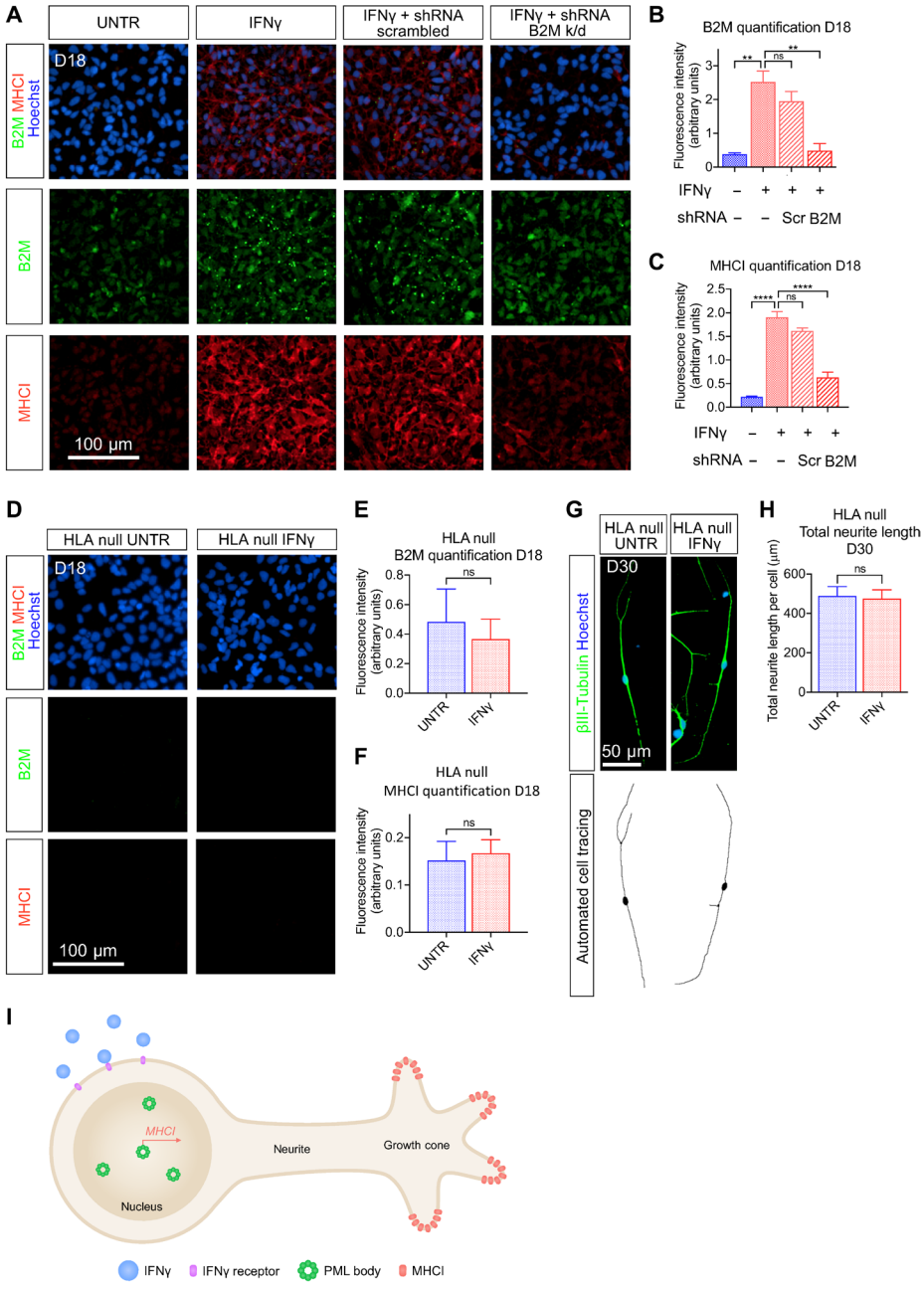

Fig. 6. Loss of B2M prevents MHCI cell surface expression and IFN-γ-dependent neurite outgrowth. (**A**) Confocal images of B2M-, MHCI-, and Hoechst-stained D18 NPCs, UNTR, IFN-γ, IFN-γ + shRNA scrambled, and IFN-γ + shRNA B2M knockdown treatment conditions. (**B** and **C**) Quantification of B2M and MHCI in D18 UNTR, IFN-γ, IFN-γ + shRNA scrambled, and IFN-γ + shRNA B2M knockdown. $n = 3$ independent biological replicates; >10,000 cells per condition; three control cell lines. One-way ANOVA with Tukey's multiple comparison correction. (**D**) Confocal images of B2M-, MHCI-, and Hoechst-stained D18 MS3 HLA null UNTR and IFN-γ-treated NPCs. (**E** and **F**) Quantification of B2M and MHCI in D18, MS3 HLA null UNTR, and IFN-γ-treated NPCs. MS3 HLA null UNTR: $n = 3$ biological replicates; >10,000 cells analyzed. MS3 HLA null IFN-γ: $n = 3$ biological replicates; >10,000 cells analyzed. Paired t test. (**G**) Fluorescence images of βIII-tubulin– and Hoechst-stained neurons and automated tracing of βIII-tubulin–stained neurites in D30 MS3 HLA null UNTR and IFN-γ neurons. (**H**) Neurite total length per cell in D30 MS3 HLA null UNTR and IFN-γ neurons. $n = 5$ independent biological replicates. MS3 HLA null UNTR, >10,000 cells analyzed; MS3 HLA null IFN-γ, >10,000 cells analyzed. Paired t test. All images and data generated using Opera Phenix high content screening system. (**I**) Schematic depicting our proposed model for IFN-γ-induced PML and MHCI-dependent neurite outgrowth. Results are presented as means ± SEM. $^{**}P < 0.01$, and $^{****}P < 0.0001$.

Furthermore, PML body disruption blocked IFN-γ-induced neurite outgrowth. While this phenomenon has not been examined before in human neurons, IFN-induced transcriptional memory has previously been observed in human cancer cells (*19*), mouse embryonic fibroblasts, and mouse bone marrow–derived macrophages (*18*). In the latter study, IFN-γ pretreated cells were shown to mount an enhanced antiviral transcriptional response, conferring resistance to viral infection (*18*). PML nuclear bodies were shown to mediate

IFN-γ-dependent transcriptional memory for the Major Histocompatibility Complex, Class II, DR Alpha (MHCII DRA) gene in human cancer cells (*19*). Building on these findings, our data indicate that IFN-γ exposure in NPCs establishes PML-dependent transcriptional memory in MHCI genes that persists through human neuronal differentiation. Both *PML* and *HLA-B* genes are up-regulated in the post-mortem ASD brain (*10*). Consistent with this, we also observed increased expression of *PML* and *HLA-B* in NPCs from a small collection of ASD-iPSCs. This indicates that this pathway may be up-regulated during development in ASD brains. Whether altered neurite outgrowth or neuronal/synaptic morphology in ASD brains is associated with elevated expression levels of PML or HLA-B requires further and detailed investigation. Moreover, these findings will need to be confirmed using a larger cohort of ASD-iPSCs generated from both syndromic and idiopathic individuals to understand if these findings could potentially be generalized to a wider population.

Genes of the MHCI complex were among the top differentially expressed in both neural progenitors and neurons following IFN-γ exposure. They exhibited evidence of transcriptional memory, where expression remained elevated in neurons that received a single IFN-γ treatment at the NPC stage. Furthermore, these genes had a heightened response to neuronal treatment when primed at the progenitor stage. Using super-resolution microscopy, we found that MHCI proteins were enriched in neuronal growth cones. Disruption of PML body formation prevented both MHCI enrichment in growth cones and IFN-γ-induced neurite outgrowth. Moreover, IFN-γ did not elicit the same neurite outgrowth phenotype in cells devoid of MHCI at the cell surface. These data indicate that MHCI proteins are involved in IFN-γ-induced neurite outgrowth. The role that MHCI proteins play in the cellular antiviral response is well established; they present antigens at the cell surface for detection by T cells. In addition, evidence is mounting for nonimmune functions in the central nervous system. MHCI proteins have been found in neurons of the developing mammalian brain, where they have been shown to localize to neurites and neuronal growth cones (*16*, *30*). They have been implicated in neurite outgrowth in mouse primary hippocampal neurons (*15*) and synaptic stability in the mouse visual system (*41*). Intriguingly, gestational poly(I:C) also leads to an enduring increase in MHCI protein in mouse cortical neurites (*20*). Note that the MHC locus has shown the strongest association with SZ in multiple GWASs (*47*, *48*); however, strong linkage disequilibrium in the region has made identifying the causal variants a challenge. Combined with the existing literature, our results indicate that MHCI proteins are involved in IFN-γ-induced neurite outgrowth. Further research is required to determine the mechanisms through which MHCI proteins alter growth cone dynamics.

A growing body of evidence indicates that genetic variants associated with SZ and ASD manifest their risk during critical periods of early brain development (*8*, *49*, *50*). Alterations in the expression and function of risk genes disturb fundamental processes involved in neuronal differentiation and maturation (*33*, *51*). In this study, we found evidence that IFN-γ exposure during human neuronal differentiation disproportionately altered the expression of genes associated with these disorders. More specifically, we found that common variants associated with SZ by GWAS significantly overlapped with genes that were down-regulated by both NPCs and neurons in response to IFN-γ. The association between IFN-γ signaling and genetic risk for SZ was supported by additional analyses of risk genes identified by the PsychENCODE consortium, which revealed enrichment in both genes down-regulated by NPCs and up-regulated by neurons in response to IFN-γ. In total, 104 of the PsychENCODE SZ risk genes responded to IFN-γ in our study. Many high profile candidates were among them, including *FOXP1*, *ATXN7*, *TSNARE1*, and *ZNF804A*. This convergence of genetic and environmental risk factors may speak to the association between maternal immune activation and SZ.

The extent to which the IFN-γ response overlaps with genetic risk for ASD is less clear. A similar association between IFN-γ-responding genes and common ASD risk variants was not found. This could be due to the fact that GWAS studies have uncovered considerably fewer genome-wide significant loci for ASD to date (*51*). As common variants are thought to represent less than 20% of genetic risk for ASD (*52*), we also carried out overlap analysis with ASD risk genes from the SFARI database that includes rare single gene mutations. We found enrichment of SFARI category 1 to 4 genes in the gene set down-regulated by NPCs in response to IFN-γ. However, this result was not supported by analysis with the shorter high confidence category 1 to 2 gene list. This inconsistency could be explained either by the reduced sample size of the shorter list reducing statistical power or by the inclusion of false positives in the broader gene list. Regardless, a total of 66 SFARI-defined ASD risk genes responded to IFN-γ in NPCs and neurons. High confidence genes such as *PTEN*, *TCF4*, *SHANK2*, *NLGN3*, and *NRXN3* were among them. *PTEN* was down-regulated in neurons after IFN-γ exposure in our study, consistent with the reduced activity caused by ASD-associated variants (*53*). This example illustrates how IFN-γ can influence risk genes in a similar manner to disease-associated genetic variants. It is not clear whether IFN-γ-responding risk genes are involved in the neurite phenotype we describe above. However, similar dysregulation in response to developmental inflammatory stimuli in vivo would be expected to have implications for brain development.

We also observed a significant overlap between genes that were differentially expressed in response to IFN-γ in our model with those found to be dysregulated in post-mortem ASD and SZ brains. The overlapping genes were enriched for genes of the IFN-γ signaling pathway and antiviral response genes. The up-regulation of immune and inflammatory factors is a consistent finding of transcriptomic studies of ASD and SZ brains (*10*). While this signal has typically been assumed to be driven by microglia, our results suggest that it may also have a neuronal origin. This observation provides validity to our model as IFN-γ alters gene expression in a manner consistent with the dysregulation observed in the brains of patients with these disorders.

In summary, we find that antiviral immune activation in human NPCs induces morphological and transcriptomic changes associated with neurodevelopmental disorders. NPCs are thought to be central to the etiology of these conditions. Their disruption can have lasting implications for neuronal migration, maturation, and function (*54*). Recently, Schafer and colleagues observed that hiPSC neurons from individuals with ASD displayed increased neurite outgrowth (*26*). They demonstrated that this phenotype was mediated by aberrant gene expression in NPCs and could be prevented by bypassing the NPC stage through direct conversion to neurons. In our study, we find that pathological priming of NPCs with IFN-γ has a similar effect. Thus, perturbation of normal gene expression in NPCs, whether genetic or environmental, leads to altered neuronal maturation. The degree to which this phenotype contributes to neurodevelopmental disorders remains an open question. Further investigation is required to determine whether the IFN-γ-responding SZ and ASD risk genes contribute to the neurite outgrowth phenotype and whether PML or MHCI mediates perturbed risk gene expression. Nonetheless,

our results highlight IFN-γ signaling as a plausible link between early immune activation and neurodevelopmental disorders. This work provides a framework for future study of immune activation and gene-environment interaction in human neural development.

MATERIALS AND METHODS

Study design

The initial objective was to determine whether IFN-γ treatment of hiPSC-NPCs followed by continued differentiation into post-mitotic neurons led to recapitulation of morphological characteristics of hiPSC neurons derived from individuals with ASD. Subsequently, we carried out RNA sequencing to determine the transcriptional changes brought about by acute treatment, pretreatment, and double treatment with IFN-γ in NPCs and neurons. We carried out gene enrichment analysis to test the hypotheses that IFN-γ would disproportionately alter the expression of SZ and ASD risk genes and those that are differentially expressed in post-mortem brains of individuals with these disorders. Further hypotheses were generated to test the requirement for PML nuclear bodies in IFN-γ-dependent MHCI transcription and the requirement for PML and MHCI in IFN-γ-dependent increased neurite outgrowth. No data were excluded from any dataset. To account for variability between cultures, multiple biological replicates were generated where appropriate and as specified. Cells from a given hiPSC line were considered to be independent biological replicates when they were generated from hiPSC samples with a different passage number. Treatments were carried out on cells within the same biological replicate, and paired or grouped statistical analysis was carried out to limit the impact of this variability on measured outcomes. The numbers of hiPSC lines and biological replicates, sample sizes, and statistical tests used are specified in figure legends. Experiment-specific parameters are outlined in the methodology sections RNA Sequencing; High content cellomic screening and Microscopy and image analysis below.

HiPSC generation and neuralization and treatment

Participants were recruited, and methods were carried out in accordance to the "Patient iPSCs for Neurodevelopmental Disorders (PiNDs) study" (REC no. 13/LO/1218). Informed consent was obtained from all subjects for participation in the PiNDs study. Ethical approval for the PiNDs study was provided by the National Health Service (NHS) Research Ethics Committee at the South London and Maudsley NHS R&D Office. HiPSCs were generated from human hair follicle keratinocytes, derived from three control males with no known psychiatric conditions and three males with diagnosed ASD (table S1). Three control hiPSC lines and one ASD hiPSC line were generated using a polycistronic lentiviral construct coexpressing the four reprogramming transcription factors, OCT4, SOX2, KLF4, and c-MYC, as previously reported (*55*). Two ASD lines were generated using CytoTune Sendai reprogramming kits (Thermo Fisher Scientific, A16517). HiPSC reprogramming was validated as previously described (*24*, *27*, *28*, *56*). Briefly, genome-wide expression profiling using Illumina BeadChip v4 and the bioinformatics tool "Pluritest" was used to confirm hiPSC identity. Pluripotency was established through differentiation into embryoid bodies, followed by immunocytochemistry for markers from the three germ layers. Expression of pluripotency markers, NANOG, OCT4, SSEA4, and TRA1-81, was confirmed by immunocytochemistry. The Illumina Human CytoSNP-12v2.1 BeadChip array and KaryoStudio analysis software (Illumina) were used to assess genome integrity (table S1).

HiPSCs were cultured in StemFlex media (Gibco, A3349401) on six-well plates (Thermo Fisher Scientific, 140675) coated with Geltrex basement membrane matrix (Thermo Fisher Scientific, A1413302). Cells were passaged upon reaching 60 to 70% confluency by incubation with a calcium chelator, EDTA (Thermo Fisher Scientific, 15040-33), followed by detachment with a cell lifter to maintain intact hiPSC colonies.

HiPSCs were differentiated as previously reported (*24*). HiPSCs were grown until 95 to 100% confluent and then neuralized using a modified dual SMAD inhibition protocol (*24*, *27*, *28*, *56*). For neuralization, StemFlex was replaced with a 1:1 mixture of N2- and B27-supplemented medium, made following the manufacturer's guidelines (Thermo Fisher Scientific, 17502048 and 17504044) to which SMAD and Wnt inhibitors (10 μM SB431542, 1 μM dorsomorphin, and 2 μM XAV939) were added (hereafter known as N2:B27+++). This was replaced daily until D7, when cells were dissociated using Accutase (Life Technologies, A11105-01) and replated at a 1:1 ratio into N2:B27+++ supplemented with Rock inhibitor (Merck, Y27632) to prevent apoptosis. From D8 onward, SMAD and WNT inhibitors were excluded from medium, and cells received daily N2:B27 medium alone. Cells were dissociated and replated on D12, D16, D19, and D21. From D9, a uniform sheet of SOX2/NESTIN-positive cells was observed (fig. S1). From D17, cells were observed to self-organize into neuroepithelial rosettes, expressing apical polarity marker PKCλ with mitotic, PH3-expressing cells located at the apical pole (fig. S1). On D21, cells were plated into poly-D-lysine–coated (5 μg/ml; Merck, P6407) and laminin–coated (20 μg/ml; Merck, L2020) plates, in B27 media, supplemented with Notch inhibitor, DAPT (*N*-[*N*-(3,5-difluorophenacetyl)-L-alanyl]-*S*-phenylglycine *t*-butyl ester), to induce cell cycle exit. From this point onward, βIII-tubulin expression and neurite extension were observed (fig. S1). Cells received IFN-γ (Abcam, AB9659) at a concentration of 25 ng/ml on D17 to D21 and D29 to D30 and As_2O_3 (Trisenox, Teva) at a concentration of 1 μM on D16 to D21, as specified.

Embryonic stem cell generation and neuralization and treatment

The hESC line MasterShef 3 HLA null was cultured as previously described for hiPSCs but using laminin LN-521–coated (5 μg/ml; BioLamina, Sweden) plates. MasterShef 3 HLA null was created using CRISPR-Cas9 nickase technology. Two plasmids containing a mutant Cas9D10A nickase plus different reporter genes green fluorescent protein (GFP) and dTomato [pSpCas9n(BB)_2A_GFP, pSpcas9n(BB)_2A_dTomato] with different guide RNAs targeting the β-2-microglobulin (*B2M*) gene were transfected into the parent line, followed by single cell sorting 4 days later for GFP/dTomato double-positive cells. Single cells were seeded onto LN-521–coated 96-well plates, and colonies were picked after 7 to 10 days. Colonies were screened by PCR for B2M expression, by flow cytometry for MHCI knockout, by T7 mismatch cleavage assay, and, lastly, by Sanger sequencing of chosen clones. hESCs were expanded and differentiated using identical protocols to hiPSC lines described above.

B2M knockdown

B2M was knocked down using lentiviral particles containing *B2M*-targeting shRNA (OriGene, TL314543V, Virus A). Nontargeting scrambled shRNA from the same kit was used as a control. Cells were exposed to the shRNA on D14 for 18 hours at a multiplicity of infection of 8. NPCs were treated with IFN-γ on D17 for 24 hours

and fixed on D18. These experiments were carried out in biological triplicate for all three control hiPSC lines.

RNA sequencing

RNA samples were collected in TRIzol reagent (Thermo Fisher Scientific, 15596026), and RNA extraction was performed using an RNEasy kit (Qiagen, 74104). Each experimental condition was repeated in the three control hiPSC lines (table S1). Libraries were prepared using the TruSeq RNA Library Preparation Kit (Illumina, RS-122-2001) by the Wellcome Trust Centre for Human Genetics, University of Oxford. Libraries were pooled and sequenced on an Illumina HiSeq 4000, resulting in an average of 38 million 75–base pair paired-end reads per sample. FASTQ files were processed with Trimmomatic (*57*) to quality trim the reads and remove adapters. The reads were then mapped to the human (GRCh38) reference genome using STAR (*58*). Count matrices were prepared using GenomicAlignments on Bioconductor (*59*), and differential gene expression analysis was carried out using the default Wald test in DESeq2 version 1.12.3 (*29*). All samples were run together using the design formula ~ cell line + treatment condition before using the contrast argument to extract the comparisons of interest. *P* values were adjusted using the Benjamini-Hochberg (BH) method, and the threshold for differential expression was a BH-adjusted $P < 0.05$. FASTQ files can be accessed from www.synapse.org/IFNG.

Gene set enrichment analysis

GO analysis was carried out with DAVID (*60*) to test for enrichment of biological process, molecular function, and cellular component. DEG lists were tested for enrichment relative to a background of all genes awarded an adjusted *P* value for that comparison by DESeq2. The threshold for enrichment was a BH-adjusted $P < 0.05$.

MAGMA 1.07b was used to test whether genes differentially expressed upon IFN-γ treatment were enriched for genes implicated in SZ or ASD according to GWAS (*31*). GWAS summary statistics were downloaded from the Walters Group Data Repository (https://walters.psycm.cf.ac.uk/) and the Psychiatric Genomics Consortium website (www.med.unc.edu/pgc/download-results/). Variants corresponding to the extended MHC region (assembly: GRCh37; location: chr6, 25,000,000–34,000,000) were excluded due to the complex linkage disequilibrium structure of this locus. MAGMA was used to identify disease-associated genes as part of a gene-level enrichment analysis step that generates gene-level association statistic adjusted for gene size, variant density, and linkage disequilibrium using the 1000 Genomes Phase 3 European reference panel. Subsequently, MAGMA was used to test whether genes differentially expressed in NPCs or neurons in association with IFN-γ treatment (split into up- and down-regulated sets) were enriched with disease-associated genes identified in the gene-level enrichment analysis. Gene-set enrichment *P* values calculated in MAGMA were corrected for eight tests (two time points, two directions of effect, and two psychiatric disorders tested) using the BH method.

Additional gene-set enrichment analysis was carried out for SZ risk genes defined by the PsychENCODE Consortium (*33*) and ASD risk genes from the SFARI database (categories 1 to 4 and categories 1 and 2, 15 January 2019 release) (*34*). None of the risk genes included in these analyses fell in the MHC region. Enrichment was tested using a two tailed Fisher's exact test in R to test whether the proportion of risk genes in the differentially expressed set is more or less than expected by chance. Thus, the two variables analyzed were differential expression status (differentially expressed versus not differentially expressed) and risk gene status (risk gene versus not risk gene). Analysis was limited to genes considered expressed in our samples according to the internal filtering criteria of DESeq2. Up- and down-regulated genes were separately tested. *P* values were corrected for 12 tests (two time points, two directions of effect, and three gene lists tested) using the BH method.

Overlap analysis was carried out between IFN-γ-responding genes detected in this study, and genes found to be DEGs from post-mortem brains of patients with ASD and SZ. The post-mortem data were from the PsychENCODE cross-disorder study, which used 559 SZ, 51 ASD, and 936 control post-mortem frontal and temporal cerebral cortex samples (*10*). Enrichment was tested using a two-tailed Fisher's exact test in R. Up- and down-regulated genes were separately tested. *P* values were corrected for eight tests (two time points, two directions of effect, and two psychiatric disorders tested) using the BH method.

Immunocytochemistry

Cells were washed in phosphate-buffered saline (PBS), fixed in 4% paraformaldehyde (20 min at room temperature), washed three times in PBS, and permeabilized and blocked using a solution of 4% donkey serum and 0.1% Triton in PBS for 1 hour at room temperature (RT). Primary antibodies (table S5) were diluted in blocking solution and applied overnight at 4°C. Following this, cells were washed three times in PBS, and appropriate Alexa Fluor secondary antibodies (A-21202, A-21203, A-21206, and A-21207, Thermo Fisher Scientific) were applied in blocking solution for 2 hours at RT. Cells were then washed three times in PBS and counterstained with Hoechst 33342 (Merck, B2261). F-actin was detected using Alexa Fluor 488–conjugated phalloidin (ActinGreen 488 ReadyProbes, Thermo Fisher Scientific, R37110) applied in PBS for 30 min following secondary antibody incubation and three washes in PBS.

High content cellomic screening

For the initial neuronal morphology experiments, high content screening was performed using CellInsight (Thermo Fisher Scientific) operated by HCS Studio Software for automated measurement of neurite outgrowth. Cells were plated at a density of 9000 cells/cm^2 in poly-D-lysine– and laminin-coated 96 well Nunclon plates (Merck, P8366), stained for βIII-tubulin (Tuj1) for detection of both mature and immature neurites and counterstained with Hoechst 33342 to detect nuclei. The analysis pipeline involved initial detection of Hoechst-stained nuclei, detection of cell bodies using nuclei as seeds, and then detection of neurites originating from cell bodies. The following features were assessed for comprehensive examination of neuronal morphology: neurite total length per cell, neurite average length per cell, neurite count per cell, and branch point count per cell. Averages were then taken for each condition within biological replicates. Identical detection parameters were used between conditions to allow direct comparison and paired statistical analysis. Analogous analysis was carried out for the MS3 HLA null hESC experiment with the Opera Phenix high content screening system (PerkinElmer). Plating and staining were carried out as described above. The Opera Phenix was also used to quantify B2M and MHCI protein levels for the *B2M* shRNAi-mediated knockdown and MS3 HLA null hESC knockout studies. In both cases, cells were fixed and stained immediately after IFN-γ treatment at D18. Protein expression was measured as average cellular intensity normalized to no-primary controls.

Quantitative PCR

RNA samples were collected in TRIzol reagent (Thermo Fisher Scientific, 15596026), and RNA extraction was performed using an RNEasy kit (Qiagen, 74104). DNA digest was performed using a TURBO DNA-free kit (Thermo Fisher Scientific, AM1907) to remove residual genomic DNA from samples. Reverse transcription to generate complementary DNA was performed using SuperScript III (Invitrogen, 18080-044). qPCR was performed using EvaGreen Hot FirePol qPCR Mix Plus (Solis Biodyne, 08-24-00001) in a Bio-Rad Chromo4 PCR detection system. qPCR primer sequences can be found in table S6. Gene expression fold changes between conditions were calculated using the comparative cycle threshold (Ct) method.

RNA FISH

RNA FISH was carried out using an RNAScope double Z probe targeting pre-splicing *HLA-B* RNA (ACD, probe named Hs-HLAB-intron). Hybridization and signal amplification were carried out using an RNAScope 2.5 HD Detection Reagent kit (ACD, 322350), following the manufacturer's instructions. Briefly, cells were grown in eight-well chamber slides (Merck, C7057), fixed in 10% neutral-buffered formalin for 30 min at RT, washed in PBS, and incubated with the probe for 2 hours at 40°C. Slides were washed, and signal was amplified through a six-step amplification process, followed by signal detection with a Fast-red chromogen label.

Microscopy and image analysis

Confocal images were taken with a Leica SP5 laser scanning confocal microscope using 405/488/594-nm lasers and a 63× [numerical aperture (NA), 1.4] oil immersion lens (Leica, Wetzlar, Germany), operated through Leica Application Suite Advanced Software (v.2.7.3). Super-resolution images were taken using a Visitech-iSIM module coupled to a Nikon Ti-E microscope with a Nikon 100× 1.49 NA total internal reflection fluorescence oil immersion lens (Nikon, Japan) using 405/488/561-nm lasers. Super-resolution images were deconvolved to increase contrast and resolution using a Richardson-Lucy algorithm specific to the iSIM mode of imaging using the supplied NIS-Elements Advanced Research software (Nikon, Japan, v.4.6). Identical laser gain and offset settings were used within each biological replicate to enable direct comparison between conditions.

Semi-automated image analysis was performed using ImageJ software. Gaussian filters were applied to PML and RNAScope images to reduce noise, and binary images were generated. Nuclei were used as boundaries within which PML and RNAScope spots were counted. Identical processing parameters were applied across conditions to allow paired or grouped statistical analysis. Numbers of PML bodies per micromolar squared were measured within RNAScope spots, within RNAScope spot perimeter regions, and within whole nuclei. RNAScope spot perimeter regions were defined as detected spot perimeters ±0.3 μm, generating a ring-shaped region of interest.

DiAna, an ImageJ plugin (*40*), was used to assess the spatial distribution of objects. Binary images were generated from confocal images of PML and RNAScope staining. Center-to-center distances were measured from PML spots to RNAScope spots. Binary images of nuclei were used as a bounding box (mask), and randomized shuffle of objects in both channels was carried out 100 times. Center-to-center distances in shuffled images were computed, and cumulated frequency distributions were calculated for real and simulated distances. This was repeated for nine images across three cell lines. Real and simulated distances within a given image were matched by percentile for paired analysis.

Data collection and statistics

Details of the statistical tests relating to differential expression and gene set enrichment are described in the "RNA sequencing" section above. All experiments were carried out using three independent iPSC lines derived from three unrelated male control or ASD-diagnosed individuals. Where possible, multiple biological replicates of each line were used (as specified in figure legends). Paired sample tests were used for data obtained from matched treated and untreated pairs of samples from the same cell line and biological replicate. Biological replicates were cultured together until 1 to 2 days before IFN-γ, As_2O_3, or combined treatment, whereupon they were passaged into separate wells. All datasets were tested for normal distribution using the D'Agostino and Pearson test before further statistical analysis. Statistical tests used for analysis of each dataset and "*n*" numbers of repeats are specified in the figure legends. Statistical tests used included *t* tests, Mann-Whitney tests, Wilcoxon matched-pairs test, Kruskal-Wallis test, and one-way and two-way ANOVAs with Tukey and Sidak's multiple comparison adjustment methods, respectively. Statistical tests used for analysis of each dataset are specified in the figure legends. RM ANOVAs were used for comparison of data from the same cell line and biological replicate. The *t* test and Mann-Whitney test were used for comparison of two groups where data were unpaired and normally or non-normally distributed, respectively. Paired *t* tests and Wilcoxon matched-pairs test were used for comparison of two groups, where data were paired and normally or non-normally distributed, respectively. Normal or RM one-way ANOVAs were performed on datasets with more than two groups, where samples were ungrouped or grouped, respectively. Normal or RM two-way ANOVAs were performed on datasets with two input variables, where samples were ungrouped or grouped, respectively. Statistical analysis was carried out using GraphPad Prism 8.

SUPPLEMENTARY MATERIALS

Supplementary material for this article is available at http://advances.sciencemag.org/cgi/content/full/6/34/eaay9506/DC1

View/request a protocol for this paper from *Bio-protocol*.

REFERENCES AND NOTES

1. M. L. Estes, A. K. Mcallister, Maternal immune activation: Implications for neuropsychiatric disorders. *Science* **353**, 772–777 (2016).
2. A. S. Brown, M. D. Begg, S. Gravenstein, C. A. Schaefer, R. J. Wyatt, Serologic evidence of prenatal influenza in the etiology of schizophrenia. *Arch. Gen. Psychiatry* **61**, 774–780 (2004).
3. M. Byrne, E. Agerbo, B. Bennedsen, W. W. Eaton, P. B. Mortensen, Obstetric conditions and risk of first admission with schizophrenia: A Danish national register based study. *Schizophr. Res.* **97**, 51–59 (2007).
4. H. Ó. Atladóttir, P. Thorsen, L. Østergaard, D. E. Schendel, S. Lemcke, M. Abdallah, E. T. Parner, Maternal infection requiring hospitalization during pregnancy and autism spectrum disorders. *J. Autism Dev. Disord.* **40**, 1423–1430 (2010).
5. H. Ó. Atladóttir, T. B. Henriksen, D. E. Schendel, E. T. Parner, Autism after infection, febrole episodes, and antibiotic use during pregancy: An exploration study. *Pediatrics* **130**, e1447–e1454 (2012).
6. U. Meyer, Prenatal Poly(I:C) exposure and other developmental immune activation models in rodent systems. *Biol. Psychiatry* **75**, 307–315 (2014).
7. I. Voineagu, X. Wang, P. Johnston, J. K. Lowe, Y. Tian, S. Horvath, J. Mill, R. M. Cantor, B. J. Blencowe, D. H. Geschwind, Transcriptomic analysis of autistic brain reveals convergent molecular pathology. *Nature* **474**, 380–384 (2011).
8. N. N. Parikshak, R. Luo, A. Zhang, H. Won, J. K. Lowe, V. Chandran, S. Horvath, D. H. Geschwind, Integrative functional genomic analyses implicate specific molecular pathways and circuits in autism. *Cell* **155**, 1008–1021 (2013).

9. S. Gupta, S. E. Ellis, F. N. Ashar, A. Moes, J. S. Bader, J. Zhan, A. B. West, D. E. Arking, Transcriptome analysis reveals dysregulation of innate immune response genes and neuronal activity-dependent genes in autism. *Nat. Commun.* **5**, 5748 (2014).
10. M. J. Gandal, P. Zhang, E. Hadjimichael, R. L. Walker, C. Chen, S. Liu, H. Won, H. Van Bakel, M. Varghese, Y. Wang, A. W. Shieh, J. Haney, S. Parhami, J. Belmont, M. Kim, P. M. Losada, Z. Khan, J. Mleczko, Y. Xia, R. Dai, D. Wang, Y. T. Yang, M. Xu, K. Fish, P. R. Hof, J. Warrell, D. Fitzgerald, K. White, A. E. Jaffe, M. A. Peters, M. Gerstein, C. Liu, L. M. Iakoucheva, D. Pinto, D. H. Geschwind, Transcriptome-wide isoform-level dysregulation in ASD, schizophrenia, and bipolar disorder. *Science* **362**, eaat8127 (2018).
11. P. A. Garay, E. Y. Hsiao, P. H. Patterson, A. K. McAllister, Maternal immune activation causes age- and region-specific changes in brain cytokines in offspring throughout development. *Brain Behav. Immun.* **31**, 54–68 (2013).
12. W. M. Schneider, M. D. Chevillotte, C. M. Rice, Interferon-stimulated genes: A complex web of host defenses. *Annu. Rev. Immunol.* **32**, 513–545 (2014).
13. P. E. Goines, L. A. Croen, D. Braunschweig, C. K. Yoshida, J. Grether, R. Hansen, M. Kharrazi, P. Ashwood, J. Van de Water, Increased midgestational IFN-γ, IL-4 and IL-5 in women bearing a child with autism: A case-control study. *Mol. Autism* **2**, 13 (2011).
14. L. S. Heuer, L. A. Croen, K. L. Jones, C. K. Yoshida, R. L. Hansen, R. Yolken, O. Zerbo, G. DeLorenze, M. Kharrazi, P. Ashwood, J. Van de Water, An exploratory examination of neonatal cytokines and chemokines as predictors of autism risk: The early markers for autism study. *Biol. Psychiatry* **86**, 255–264 (2019).
15. T. Bilousova, H. Dang, W. Xu, S. Gustafson, Y. Jin, L. Wickramasinghe, T. Won, G. Bobarnac, B. Middleton, J. Tian, D. L. Kaufman, Major histocompatibility complex class I molecules modulate embryonic neuritogenesis and neuronal polarization. *J. Neuroimmunol.* **247**, 1–8 (2012).
16. L. A. Needleman, X.-B. Liu, F. El-Sabeawy, E. G. Jones, A. K. McAllister, MHC class I molecules are present both pre- and postsynaptically in the visual cortex during postnatal development and in adulthood. *Proc. Natl. Acad. Sci. U.S.A.* **107**, 16999–17004 (2010).
17. A. J. Filiano, Y. Xu, N. J. Tustison, R. L. Marsh, W. Baker, I. Smirnov, C. C. Overall, S. P. Gadani, S. D. Turner, Z. Weng, S. N. Peerzade, H. Chen, K. S. Lee, M. M. Scott, M. P. Beenhakker, V. Litvak, J. Kipnis, Unexpected role of interferon-γ in regulating neuronal connectivity and social behaviour. *Nature* **535**, 425–429 (2016).
18. R. Kamada, W. Yang, Y. Zhang, M. C. Patel, Y. Yang, R. Ouda, A. Dey, Y. Wakabayashi, K. Sakaguchi, T. Fujita, T. Tamura, J. Zhu, K. Ozato, Interferon stimulation creates chromatin marks and establishes transcriptional memory. *Proc. Natl. Acad. Sci. U.S.A.* **115**, E9162–E9171 (2018).
19. M. Gialitakis, P. Arampatzi, T. Makatounakis, J. Papamatheakis, Gamma interferon-dependent transcriptional memory via relocalization of a gene locus to PML nuclear bodies. *Mol. Cell. Biol.* **30**, 2046–2056 (2010).
20. B. M. Elmer, M. L. Estes, S. L. Barrow, A. K. McAllister, MHCI requires MEF2 transcription factors to negatively regulate synapse density during development and in disease. *J. Neurosci.* **33**, 13791–13804 (2013).
21. E. Korb, C. L. Wilkinson, R. N. Delgado, K. L. Lovero, S. Finkbeiner, Arc in the nucleus regulates PML-dependent GluA1 transcription and homeostatic plasticity. *Nat. Neurosci.* **16**, 874–883 (2013).
22. T. Regad, C. Bellodi, P. Nicotera, P. Salomoni, The tumor suppressor Pml regulates cell fate in the developing neocortex. *Nat. Neurosci.* **12**, 132–140 (2009).
23. Y. Li, G. Missig, B. C. Finger, S. M. Landino, A. J. Alexander, E. L. Mokler, J. O. Robbins, Y. Manasian, W. Kim, K.-S. Kim, C. J. McDougle, W. A. Carlezon Jr., V. Y. Bolshakov, Maternal and early postnatal immune activation produce dissociable effects on neurotransmission in mPFC–amygdala circuits. *J. Neurosci.* **38**, 3358–3372 (2018).
24. A. Kathuria, P. Nowosiad, R. Jagasia, S. Aigner, R. D. Taylor, L. C. Andreae, N. J. F. Gatford, W. Lucchesi, D. P. Srivastava, J. Price, Stem cell-derived neurons from autistic individuals with SHANK3 mutation show morphogenetic abnormalities during early development. *Mol. Psychiatry* **23**, 735–746 (2018).
25. A. Deshpande, S. Yadav, D. Q. Dao, Z.-Y. Wu, K. C. Hokanson, M. K. Cahill, A. P. Wiita, Y.-N. Jan, E. M. Ullian, L. A. Weiss, Cellular phenotypes in human iPSC-derived neurons from a genetic model of autism spectrum disorder. *Cell Rep.* **21**, 2678–2687 (2017).
26. S. T. Schafer, A. C. M. Paquola, S. Stern, D. Gosselin, M. Ku, M. Pena, T. J. M. Kuret, M. Liyanage, A. A. Mansour, B. N. Jaeger, M. C. Marchetto, C. K. Glass, J. Mertens, F. H. Gage, Pathological priming causes developmental gene network heterochronicity in autistic subject-derived neurons. *Nat. Neurosci.* **22**, 243–255 (2019).
27. C. Shum, L. Dutan, E. Annuario, K. Warre-Cornish, S. E. Taylor, R. D. Taylor, L. C. Andreae, N. J. Buckley, J. Price, S. Bhattacharyya, D. P. Srivastava, Δ^9-tetrahydrocannabinol and 2-AG decreases neurite outgrowth and differentially affects ERK1/2 and Akt signaling in hiPSC-derived cortical neurons. *Mol. Cell. Neurosci.* **103**, 103463 (2020).
28. P. J. M. Deans, P. Raval, K. J. Sellers, N. J. F. Gatford, S. Halai, R. R. R. Duarte, C. Shum, K. Warre-Cornish, V. E. Kaplun, G. Cocks, M. Hill, N. J. Bray, J. Price, D. P. Srivastava, Psychosis risk candidate ZNF804A localizes to synapses and regulates neurite formation and dendritic spine structure. *Biol. Psychiatry* **82**, 49–61 (2017).
29. M. I. Love, W. Huber, S. Anders, Moderated estimation of fold change and dispersion for RNA-seq data with DESeq2. *Genome Biol.* **15**, 550 (2014).
30. M. W. Glynn, B. M. Elmer, P. A. Garay, X.-B. Liu, L. A. Needleman, F. El-Sabeawy, A. K. McAllister, MHCI negatively regulates synapse density during the establishment of cortical connections. *Nat. Neurosci.* **14**, 442–451 (2012).
31. C. A. de Leeuw, J. M. Mooij, T. Heskes, D. Posthuma, MAGMA: Generalized gene-set analysis of GWAS data. *PLOS Comput. Biol.* **11**, e1004219 (2015).
32. A. F. Pardiñas, P. Holmans, A. J. Pocklington, V. Escott-Price, S. Ripke, N. Carrera, S. E. Legge, S. Bishop, D. Cameron, M. L. Hamshere, J. Han, L. Hubbard, A. Lynham, K. Mantripragada, E. Rees, J. H. Mac Cabe, S. A. McCarroll, B. T. Baune, G. Breen, E. M. Byrne, U. Dannlowski, T. C. Eley, C. Hayward, N. G. Martin, A. M. McIntosh, R. Plomin, D. J. Porteous, N. R. Wray, A. Caballero, D. H. Geschwind, L. M. Huckins, D. M. Ruderfer, E. Santiago, P. Sklar, E. A. Stahl, H. Won, E. Agerbo, T. D. Als, O. A. Andreassen, M. Bækvad-Hansen, P. B. Mortensen, C. B. Pedersen, A. D. Børglum, J. Bybjerg-Grauholm, S. Djurovic, N. Durmishi, M. G. Pedersen, V. Golimbet, J. Grove, D. M. Hougaard, M. Mattheisen, E. Molden, O. Mors, M. Nordentoft, M. Pejovic-Milovancevic, E. Sigurdsson, T. Silagadze, C. S. Hansen, K. Stefansson, H. Stefansson, S. Steinberg, S. Tosato, T. Werge; GERAD Consortium; CRESTAR Consortium, D. A. Collier, D. Rujescu, G. Kirov, M. J. Owen, M. C. O'Donovan, J. T. R. Walters, Common schizophrenia alleles are enriched in mutation-intolerant genes and in regions under strong background selection. *Nat. Genet.* **50**, 381–389 (2018).
33. D. Wang, S. Liu, J. Warrell, H. Won, X. Shi, F. C. P. Navarro, D. Clarke, M. Gu, P. Emani, Y. T. Yang, M. Xu, M. J. Gandal, S. Lou, J. Zhang, J. J. Park, C. Yan, S. K. Rhie, K. Manakongtreecheep, H. Zhou, A. Nathan, M. Peters, E. Mattei, D. Fitzgerald, T. Brunetti, J. Moore, Y. Jiang, K. Girdhar, G. E. Hoffman, S. Kalayci, Z. H. Gümüş, G. E. Crawford; Psych ENCODE Consortium, P. Roussos, S. Akbarian, A. E. Jaffe, K. P. White, Z. Weng, N. Sestan, D. H. Geschwind, J. A. Knowles, M. B. Gerstein, Comprehensive functional genomic resource and integrative model for the human brain. *Science* **362**, eaat8464 (2018).
34. B. S. Abrahams, D. E. Arking, D. B. Campbell, H. C. Mefford, E. M. Morrow, L. A. Weiss, I. Menashe, T. Wadkins, S. Banerjee-basu, A. Packer, SFARI Gene 2.0: A community-driven knowledgebase for the autism spectrum disorders (ASDs). *Mol. Autism* **4**, 36 (2013).
35. N. Masroori, N. Merindol, L. Berthoux, The interferon-induced antiviral protein PML (TRIM19) promotes the restriction and transcriptional silencing of lentiviruses in a context-specific, isoform-specific fashion. *Retrovirology* **13**, 19 (2016).
36. X.-W. Zhang, X.-J. Yan, Z.-R. Zhou, F.-F. Yang, Z.-Y. Wu, H.-B. Sun, W.-X. Liang, A.-X. Song, V. Lallemand-Breitenbach, M. Jeanne, Q.-Y. Zhang, H.-Y. Yang, Q.-H. Huang, G.-B. Zhou, J.-H. Tong, Y. Zhang, J.-H. Wu, H.-Y. Hu, H. de Thé, S.-J. Chen, Z. Chen, Arsenic trioxide controls the fate of the PML-RARα oncoprotein by directly binding PML. *Science* **328**, 240–243 (2010).
37. M. V. Lombardo, H. M. Moon, J. Su, T. D. Palmer, E. Courchesne, T. Pramparo, Maternal immune activation dysregulation of the fetal brain transcriptome and relevance to the pathophysiology of autism spectrum disorder. *Mol. Psychiatry* **23**, 1001–1013 (2018).
38. E. Loth, T. Charman, L. Mason, J. Tillmann, E. J. H. Jones, C. Wooldridge, J. Ahmad, B. Auyeung, C. Brogna, S. Ambrosino, T. Banaschewski, S. Baron-Cohen, S. Baumeister, C. Beckmann, M. Brammer, D. Brandeis, S. Bölte, T. Bourgeron, C. Bours, Y. de Bruijn, B. Chakrabarti, D. Crawley, I. Cornelissen, F. Dell' Acqua, G. Dumas, S. Durston, C. Ecker, J. Faulkner, V. Frouin, P. Garces, D. Goyard, H. Hayward, L. M. Ham, J. Hipp, R. J. Holt, M. H. Johnson, J. Isaksson, P. Kundu, M.-C. Lai, X. L. D'ardhuy, M. V. Lombardo, D. J. Lythgoe, R. Mandl, A. Meyer-Lindenberg, C. Moessnang, N. Mueller, L. O'Dwyer, M. Oldehinkel, B. Oranje, G. Pandina, A. M. Persico, A. N. V. Ruigrok, B. Ruggeri, J. Sabet, R. Sacco, A. San José Cáceres, E. Simonoff, R. Toro, H. Tost, J. Waldman, S. C. R. Williams, M. P. Zwiers, W. Spooren, D. G. M. Murphy, J. K. Buitelaar, The EU-AIMS Longitudinal European Autism Project (LEAP): Design and methodologies to identify and validate stratification biomarkers for autism spectrum disorders. *Mol. Autism* **8**, 24 (2017).
39. T. Alpert, L. Herzel, K. M. Neugebauer, Perfect timing: Splicing and transcription rates in living cells. *Wiley Interdiscip. Rev. RNA* **8**, e1401 (2017).
40. J. F. Gilles, M. Dos Santos, T. Boudier, S. Bolte, N. Heck, DiAna, an ImageJ tool for object-based 3D co-localization and distance analysis. *Methods* **115**, 55–64 (2017).
41. J. Syken, T. GrandPre, P. O. Kanold, C. J. Shatz, PirB restricts ocular-dominance plasticity in visual cortex. *Science* **313**, 11795–11800 (2006).
42. G. Wong, Y. Goldshmit, A. M. Turnley, Interferon-γ but not TNFα promotes neuronal differentiation and neurite outgrowth of murine adult neural stem cells. *Exp. Neurol.* **187**, 171–177 (2004).
43. J. H. Song, C. X. Wang, D. K. Song, P. Wang, A. Shuaib, C. Hao, Interferon γ induces neurite outgrowth by up-regulation of p35 neuron-specific cyclin-dependent kinase 5 activator via activation of ERK1/2 pathway. *J. Biol. Chem.* **280**, 12896–12901 (2005).
44. K. J. Brennand, A. Simone, J. Jou, C. Gelboin-Burkhart, N. Tran, S. Sangar, Y. Li, Y. Mu, G. Chen, D. Yu, S. McCarthy, J. Sebat, F. H. Gage, Modelling schizophrenia using human induced pluripotent stem cells. *Nature* **473**, 221–225 (2011).
45. V. A. Kulkarni, B. L. Firestein, The dendritic tree and brain disorders. *Mol. Cell. Neurosci.* **50**, 10–20 (2012).

46. Y.-N. Jan, L. Y. Jan, Branching out: Mechanisms of dendritic arborization. *Nat. Rev. Neurosci.* **11**, 316–328 (2010).
47. Schizophrenia Working Group of the Psychiatric Genomics Consortium, Biological insights from 108 schizophrenia-associated genetic loci. *Nature* **511**, 421–427 (2014).
48. J. Shi, D. F. Levinson, J. Duan, A. R. Sanders, Y. Zheng, I. Pe'er, F. Dudbridge, P. A. Holmans, A. S. Whittemore, B. J. Mowry, A. Olincy, F. Amin, C. R. Cloninger, J. M. Silverman, N. G. Buccola, W. F. Byerley, D. W. Black, R. R. Crowe, J. R. Oksenberg, D. B. Mirel, K. S. Kendler, R. Freedman, P. V. Gejman, Common variants on chromosome 6p22.1 are associated with schizophrenia. *Nature* **460**, 753–757 (2009).
49. M. J. Hill, J. G. Donocik, R. A. Nuamah, C. A. Mein, R. Sainz-Fuertes, N. J. Bray, Transcriptional consequences of schizophrenia candidate miR-137 manipulation in human neural progenitor cells. *Schizophr. Res.* **153**, 225–230 (2014).
50. A. E. Jaffe, R. E. Straub, J. H. Shin, R. Tao, Y. Gao, L. Collado-Torres, T. Kam-Thong, H. S. Xi, J. Quan, Q. Chen, C. Colantuoni, W. S. Ulrich, B. J. Maher, A. Deep-Soboslay; The Brain Seq Consortium, A. J. Cross, N. J. Brandon, J. T. Leek, T. M. Hyde, J. E. Kleinman, D. R. Weinberger, Developmental and genetic regulation of the human cortex transcriptome illuminate schizophrenia pathogenesis. *Nat. Neurosci.* **21**, 1117–1125 (2018).
51. J. Grove, S. Ripke, T. D. Als, M. Mattheisen, R. K. Walters, H. Won, J. Pallesen, E. Agerbo, O. A. Andreassen, R. Anney, S. Awashti, R. Belliveau, F. Bettella, J. D. Buxbaum, J. Bybjerg-Grauholm, M. Bækvad-Hansen, F. Cerrato, K. Chambert, J. H. Christensen, C. Churchhouse, K. Dellenvall, D. Demontis, S. De Rubeis, B. Devlin, S. Djurovic, A. L. Dumont, J. I. Goldstein, C. S. Hansen, M. E. Hauberg, M. V. Hollegaard, S. Hope, D. P. Howrigan, H. Huang, C. M. Hultman, L. Klei, J. Maller, J. Martin, A. R. Martin, J. L. Moran, M. Nyegaard, T. Nærland, D. S. Palmer, A. Palotie, C. B. Pedersen, M. G. Pedersen, T. dPoterba, J. B. Poulsen, B. S. Pourcain, P. Qvist, K. Rehnström, A. Reichenberg, J. Reichert, E. B. Robinson, K. Roeder, P. Roussos, E. Saemundsen, S. Sandin, F. K. Satterstrom, G. D. Smith, H. Stefansson, S. Steinberg, C. R. Stevens, P. F. Sullivan, P. Turley, G. B. Walters, X. Xu; Autism Spectrum Disorder Working Group of the Psychiatric Genomics Consortium; BUPGEN; Major Depressive Disorder Working Group of the Psychiatric Genomics Consortium; 23andMe Research Team, K. Stefansson, D. H. Geschwind, M. Nordentoft, D. M. Hougaard, T. Werge, O. Mors, P. B. Mortensen, B. M. Neale, M. J. Daly, A. D. Børglum, Identification of common genetic risk variants for autism spectrum disorder. *Nat. Genet.* **51**, 431–444 (2019).
52. The Brainstorm Consortium, Analysis of shared heritability in common disorders of the brain. *Science* **360**, eaap8757 (2018).
53. A. Orrico, L. Galli, S. Buoni, A. Orsi, G. Vonella, V. Sorrentino, Novel *PTEN* mutations in neurodevelopmental disorders and macrocephaly. *Clin. Genet.* **75**, 195–198 (2009).
54. R. Stoner, M. L. Chow, M. P. Boyle, S. M. Sunkin, P. R. Mouton, S. Roy, A. Wynshaw-Boris, S. A. Colamarino, E. S. Lein, E. Courchesne, Patches of disorganization in the neocortex of children with autism. *N. Engl. J. Med.* **370**, 1209–1219 (2014).
55. G. Cocks, S. Curran, P. Gami, D. Uwanogho, A. R. Jeffries, A. Kathuria, W. Lucchesi, V. Wood, R. Dixon, C. Ogilvie, T. Steckler, J. Price, The utility of patient specific induced pluripotent stem cells for the modelling of Autistic Spectrum Disorders. *Psychopharmacology (Berl)* **231**, 1079–1088 (2014).
56. D. Adhya, V. Swarup, R. Nagy, C. Shum, P. Nowosiad, K. M. Jozwik, I. Lee, D. Skuse, F. A. Flinter, G. McAlonan, M. A. Mendez, J. Horder, D. Murphy, D. H. Geschwind, J. Price, J. Carroll, D. P. Srivastava, S. Baron-Cohen, Atypical neurogenesis in induced pluripotent stem cell (iPSC) from autistic individuals. *Biol. Psychiatry* 10.1016/j.biopsych.2020.06.014, (2019).
57. A. M. Bolger, M. Lohse, B. Usadel, Trimmomatic: A flexible trimmer for Illumina sequence data. *Bioinformatics* **30**, 2114–2120 (2014).
58. A. Dobin, C. A. Davis, F. Schlesinger, J. Drenkow, C. Zaleski, S. Jha, P. Batut, M. Chaisson, T. R. Gingeras, STAR: Ultrafast universal RNA-seq aligner. *Bioinformatics* **29**, 15–21 (2013).
59. M. Lawrence, W. Huber, H. Pagès, P. Aboyoun, M. Carlson, R. Gentleman, M. T. Morgan, V. J. Carey, Software for computing and annotating genomic ranges. *PLOS Comput. Biol.* **9**, e1003118 (2013).
60. D. W. Huang, B. T. Sherman, R. A. Lempicki, Systematic and integrative analysis of large gene lists using DAVID bioinformatics resources. *Nat. Protoc.* **4**, 44–57 (2009).

Acknowledgments: We thank the Wohl Cellular Imaging Centre (WCIC) at the IoPPN, King's College, London, for help with microscopy. We would like to thank N. Bray (Cardiff University) and R. Sorrentino (Sapienza University of Rome) for critical discussions on this manuscript. **Funding:** The study was supported by grants from the European Autism Interventions (EU-AIMS) and AIMS-2-TRIALS: EU-AIMS received support from the IMI Joint Undertaking (JU) under grant agreement no.115300, resources of which are composed of financial contribution from the European Union's Seventh Framework Programme (FP7/2007-2013), from the European Federation of Pharmaceutical Industries and Associations (EFPIA) companies' in kind contribution, and from Autism Speaks (to J.P., D.P.S., G.M., and G.M.). AIMS-2-TRIALS received funding from the IMI 2 JU under grant agreement no. 777394. The JU receives support from the European Union's Horizon 2020 research and innovation programme and EFPIA, Autism Speaks, Autistica, and the Simons Foundation Autism Research Initiative (to G.M. and D.M.); StemBANCC: support from the Innovative Medicines Initiative joint undertaking under grant 115439-2, whose resources are composed of financial contribution from the European Union (FP7/2007-2013) and EFPIA companies' in-kind contribution (to J.P. and D.P.S.); and MATRICS: the European Union's Seventh Framework Programme (FP7-HEALTH-603016) (to D.P.S. and J.P.). In addition, funds from the Wellcome Trust ISSF Grant (no. 097819) and the King's Health Partners Research and Development Challenge Fund, a fund administered on behalf of King's Health Partners by Guy's and St Thomas' Charity awarded to D.P.S., and the Brain and Behavior Foundation [formally National Alliance for Research on Schizophrenia and Depression (NARSAD); grant no. 25957] awarded to D.P.S. were used to support this study. **Author contributions:** K.W.-C., L.P., R.N., R.R.R.D., M.J.R., P.R., and A.C. carried out all experiments, performed data analysis, or generated iPSC lines. A.M., A.L.E., and C.G. produced the gene-edited MS3 HLA null hESC line. G.M. and E.L. identified patients and obtained clinical data. D.M. supervised the studies where iPSC lines were collected. T.R.P., A.C.V., D.P.S., and J.P. supervised all experiments. K.W.-C., L.P., T.R.P., A.C.V., D.P.S., and J.P. drafted the manuscript. D.P.S. and J.P. oversaw the project. D.P.S. finalized the manuscript. **Competing interests:** The authors declare that they have no competing interests. **Data and materials availability:** All data needed to evaluate the conclusions in the paper are present in the paper and/or the Supplementary Materials. Additional data related to this paper may be requested from the authors. RNA sequencing data can be found at www.synapse.org/IFNG.

Submitted 1 October 2019
Accepted 7 July 2020
Published 19 August 2020
10.1126/sciadv.aay9506

Citation: K. Warre-Cornish, L. Perfect, R. Nagy, R. R. Duarte, M. J. Reid, P. Raval, A. Mueller, A. L. Evans, A. Couch, C. Ghevaert, G. McAlonan, E. Loth, D. Murphy, T. R. Powell, A. C. Vernon, D. P. Srivastava, J. Price, Interferon-γ signaling in human iPSC–derived neurons recapitulatesneurodevelopmental disorder phenotypes. *Sci. Adv.* **6**, eaay9506 (2020).